Silencing the Giant: Evidence of AGN Feedback and Quenching in a Little Red Dot at z = 4.13

Vasily Kokorev, ¹ John Chisholm, ¹ Ryan Endsley, ¹ Steven L. Finkelstein, ¹ Jenny E. Greene, ² Hollis B. Akins, ¹ Volker Bromm, ¹ Caitlin M. Casey, ¹ Seiji Fujimoto, ^{1,3} Ivo Labbé, ⁴ and Rebecca L. Larson⁵

Department of Astronomy, The University of Texas at Austin, Austin, TX 78712, USA
 Department of Astrophysical Sciences, Princeton University, 4 Ivy Lane, Princeton, NJ 08544
 Cosmic Dawn Center (DAWN), Niels Bohr Institute, University of Copenhagen, Jagtvej 128, København N, DK-2200, Denmark
 Centre for Astrophysics and Supercomputing, Swinburne University of Technology, Melbourne, VIC 3122, Australia
 School of Physics and Astronomy, Rochester Institute of Technology, 84 Lomb Memorial Drive, Rochester, NY 14623, USA

(Received n/a; Revised n/a; Accepted n/a)

Submitted to ApJ

ABSTRACT

The James Webb Space Telescope (JWST) has uncovered a ubiquitous population of dust-obscured compact sources at $z \gtrsim 4$. Many of these objects exhibit signs of active galactic nucleus (AGN) activity, making their study crucial for understanding the formation of supermassive black holes (SMBHs) and their growth with host galaxies. In this work, we examine low and medium resolution JWST/NIRSpecspectra from the JADES GTO public data release in the GOODS-N field of a red, luminous ($M_{\rm B} \sim$ -22.2 mag) and compact (< 500 pc) source at z = 4.13. The rest-optical ($\lambda_{\rm rest} > 4000$ Å) continuum of this source is strongly dominated by a massive ($\log_{10}[M_*/M_{\odot}] \sim 10.6$), quenched ($\log_{10}[\text{sSFR/yr}^{-1}]$ <-11) galaxy, as indicated by the clear presence of a Balmer break and stellar absorption lines. Starformation history modeling reveals a starburst episode followed by rapid quenching about 200 Myr ago. The spectrum shows extremely broad (FWHM $\sim 2500 \text{ km/s}$) H α emission and elevated optical line ratios, indicating an actively accreting SMBH. Moreover, our work has potentially revealed clear AGN signatures in the rest-UV in LRDs for the first time, via a detection of a strong Ly α emission and a broad Mg II doublet. The derived black hole mass of $\log_{10}(M_{\rm BH}/M_{\odot}) \sim 7.3$ results in $M_{\rm BH}/M_{*} \sim 0.04$ %, consistent with the local relations, unlike the elevated ratios in other high-z reddened AGN. Finally, we use JWST data from AGN at z = 4 - 10 to explore an evolutionary link between high-z reddened AGN, early quiescent galaxies, and local ellipticals.

Keywords: Active galactic nuclei (16), High-redshift galaxies (734), Early universe (435), Galaxy quenching (2040), Quenched galaxies (2016),

1. INTRODUCTION

Observations over the past few decades have established that super massive black holes (SMBHs) exist in the cores of nearly all massive galaxies locally (Kormendy et al. 1997; Richstone et al. 1998; Kormendy & Ho 2013). The growth of SMBHs is driven by gas accretion, designating such black holes as an active galactic nucleus (AGN). Powerful AGN drive the energy and momentum in the interstellar medium (ISM) of galaxies,

Corresponding author: Vasily Kokorev vkokorev@utexas.edu

heating up the gas and slowing down star formation. As such the growth of stars in galaxies and the physics of their SMBHs are tightly linked (Heckman & Best 2014).

The James Webb Space Telescope (JWST) is at the center stage of discovery of high-z AGN, getting ever closer to their epoch of formation. The first two years of its operation have marked a discovery of numerous, previously-missing, UV-faint AGN, shifting our paradigm of SMBH formation (Smith & Bromm 2019). These have been identified through a combination of directly observing broad lines (Type I; Goulding et al. 2023; Harikane et al. 2023; Juodžbalis et al. 2024; Kocevski et al. 2023; Larson et al. 2023; Maiolino et al. 2023a,b; Matthee et al. 2023; Übler et al. 2023), inferring

their AGN nature through ionization (Type II; Chisholm et al. 2024; Scholtz et al. 2023), or some combination of color and morphology (Barro et al. 2023; Iani et al. 2024; Yang et al. 2023).

Among these, an enigmatic population of compact red sources, so called "little red dots" (LRDs; Matthee et al. 2023), stands out in particular. These show a characteristic double-break feature in their spectral energy distributions (SEDs), with seemingly dust-free UV emission and a steep red slope in the rest-optical (Furtak et al. 2023; Kocevski et al. 2023; Labbé et al. 2023a). These were initially speculated to be massive compact galaxies at early epochs (Barro et al. 2023; Labbé et al. 2023b), however spectroscopic follow-up observations in many of these sources have shown clear evidence of broad Balmer emission and high-ionization, all implicating them as actively accreting SMBHs (Fujimoto et al. 2023; Furtak et al. 2024; Greene et al. 2024; Killi et al. 2023; Kocevski et al. 2023; Kokorev et al. 2023a; Matthee et al. 2023; Übler et al. 2023).

Staggeringly, SMBHs in a large number of high-z AGN, including LRDs, are overmassive, with the ratio between their black hole and stellar mass $(M_{\rm BH}/M_*)$ reaching upwards of $\sim 30 - 50 \%$ (Bogdan et al. 2023; Goulding et al. 2023; Juodžbalis et al. 2024; Kokorev et al. 2023a) which significantly deviates from the local relations (e.g. Greene et al. 2016) by more than a few orders of magnitude (Pacucci et al. 2023; Pacucci & Loeb 2024). Seemingly the growth of these black holes completely outpaces that of their host galaxies, at least at early times (e.g., Jeon et al. 2024). In contrast, quite a few of these systems have been shown to be fully consistent with the local $M_{\rm BH} - \sigma$ relations (Maiolino et al. 2023b), which could point toward the presence of gas reservoirs that sustain the growth of the central AGN, but which are inefficient at forming stars.

Detailed spectroscopic (Greene et al. 2024; Maiolino et al. 2023b; Matthee et al. 2023) and photometric (Akins et al. 2024; Kocevski et al. 2024; Kokorev et al. 2024) forays into their number densities reveal LRDs to be much more abundant compared to the UV-selected quasars at $z \sim 4-6$. They appear to account for a significant fraction of all broad-line selected AGN (Harikane et al. 2023) and even for a few percent of the total galaxy population at z > 6. The over-abundance of AGN with large BH masses relative to local scaling relations in the first few billion years of cosmic evolution can therefore truly test our models and preconceived vision of BH seeding as well as their evolution alongside their host galaxies (Dayal et al. 2024; Dayal 2024; Natarajan et al. 2023).

What has yet remained unclear is the origin of the observed rest-UV emission in LRDs. So far, the interpretations range from scattered light from the AGN itself or an unobscured host galaxy component (Akins et al. 2023; Barro et al. 2023; Greene et al. 2024; Kocevski et al. 2023, 2024; Labbé et al. 2023a). Given the similarities between the observed UV slopes of quasars and starforming galaxies, neither deep JWST spectra (Greene et al. 2024; Kokorev et al. 2023a), nor vast photometric samples of LRDs (Akins et al. 2024; Kocevski et al. 2024; Kokorev et al. 2024) have been able to make a conclusive determination. Lacking a complete understanding of the rest-UV side of LRDs prevents us from robustly deriving properties such as the stellar mass (M_*) , star formation rate (SFR), dust attenuation $(A_{\rm V})$ and ionization state in these sources. This in turn limits our ability to attain an accurate view of the impact the AGN has on its host.

Finally, despite hiding behind a thick veil of dust, these objects can be quite bright, sometimes reaching observed F444W magnitudes of 22 - 23 (Akins et al. 2024; Kokorev et al. 2024; Wang et al. 2024; Labbé et al. in prep.), and yet a similar class of objects has not been detected at either intermediate ($z \leq 4$) redshifts or locally (Kocevski et al. 2024). Seemingly this complete absence of overmassive SMBHs at late times implies that such AGN only exist at early times and on short timescales, followed by an uncertain descendant population. Recent works by Wang et al. (2024) and Labbé et al. (in prep.) show that some reddened broadline (BL) AGN already have quite evolved stellar populations by $z \sim 4$, as implied by their strong Balmer breaks and absorption lines. Therefore, older LRDs may be positioned more in line with quiescent galaxies found at similar redshifts (Carnall et al. 2023; de Graaff et al. 2024), rather than extreme AGN at high-z. Could this be the next step of overmassive SMBH evolution?

In this work, we report the discovery of BL AGN emission in an otherwise stellar dominated galaxy at z = 4.13. The deep JWST/NIRSpec Micro-Shutter Assembly (MSA) PRISM and medium resolution grating spectra in the GOODS-N field (D'Eugenio et al. 2024), allow us to identify the presence of a broad $H\alpha$ emission alongside an an array of [O III], [N II] and [S II] lines, all showing line ratios typical for AGN activity. At the same time, we also observe a strong Balmer break and a multitude of Balmer absorption lines indicative of an evolved stellar population. While this galaxy is completely consistent with the little red dot (LRD) color and compactness criteria, the observed red rest-optical color likely originates from an evolved stellar population, rather than from the reddened AGN continuum emission. Through the examination of black hole to host mass ratio we conclude that GN-72127 has more in common with quiescent galaxies (Carnall et al. 2023; de Graaff et al. 2024) and local ellipticals rather than the extreme high-z AGN observed with JWST. Using that information we attempt to draw an evolutionary sequence that connects objects with elevated $M_{\rm BH}/M_*$ at high-z to the evolved galaxies with residual AGN activity we observe later on. Moreover, our work has potentially revealed clear AGN signatures in the rest-UV in LRDs for the first time, via a detection of a strong Ly α emission and a broad Mg II doublet. We present the data in Section 2, line and continuum fitting as well as size measurements in Section 3, galaxy and black hole properties in Section 4, and the final discussion in Section 5.

Throughout this work we assume a flat Λ CDM cosmology (e.g. Planck Collaboration et al. 2020) with $\Omega_{\rm m,0}=0.3,~\Omega_{\Lambda,0}=0.7$ and $H_0=70~{\rm km~s^{-1}~Mpc^{-1}},$ and a Chabrier (2003) initial mass function (IMF) between $0.1-100~M_{\odot}$. All magnitudes are expressed in the AB system (Oke 1974).

2. OBSERVATIONS AND DATA

In our work we use the data obtained as a part of the *JWST* Advanced Deep Extragalactic Survey (JADES; Bunker et al. 2023; Eisenstein et al. 2023a,b), which is based on more than 770 hours of the GTO time with the NIRCam and NIRSpec instruments. In particular, we focus our efforts on the public JADES Data Release 3 (DR3), which covers the GOODS-North field (Giavalisco et al. 2004) and includes the NIRCam coverage in 7 broad-band (F090W, F115W, F150W, F200W, F277W, F356W, F444W) and 2 medium-band (F335M, F410M) filters. The data are fully publicly available, including the reduced spectra and catalogs¹.

Most pertinent to our work, this field was targeted by NIRSpec Multi-Shutter Array (MSA) over 4 separate MSA observations. Briefly, each observation consisted of 3 pointings, each with a small spatial offset and used the PRISM ($R \sim 100$), G140M, G235M and G395M ($R \sim 1000$) gratings. Observations used in our work were completed between April and May 2023. Details concerning both the photometric and spectroscopic data reduction, calibration and extraction of the spectra can be found in Bunker et al. (2023) and D'Eugenio et al. (2024).

We, however, would like to note a few crucial details. Factors such as path-loss correction, flux calibration uncertainty, slit position, source location within the slit, and source self-subtraction can affect the normalization, especially when combining observations from multiple MSA pointings. To address this, the JADES team has rescaled the spectra by convolving the 1D spectra with all NIRCam filters and correcting them by fitting a first-order polynomial to the ratio between NIRCam and convolved NIRSpec flux densities (similar to Greene et al. 2024; Kokorev et al. 2023a; Price et al., in prep). We verified the consistency between photometry (D'Eugenio et al. 2024) and spectra for all dispersers, and find the results satisfactory.

Second, the MSA configuration employed by the JADES team allows for the contamination of the spectra by other objects in the same detector row. However, for bright objects with multiple line detections, and robust spectroscopic redshifts, the contaminant lines are easy to identify and mask out.

3. DATA ANALYSIS

The data from JADES in the GOODS-N field are excellently suited to explore the enigmatic rest-frame UV emission of compact obscured AGN. The available JWST photometry covers a complete wavelength range from $0.4-5~\mu\mathrm{m}$, in 7 broad and 2 medium bands, reaching a median 5σ depth of 29.4 AB mag in F444W filter allowing for robust target pre-selection. Moreover, the exquisite coverage provided by all 3 medium resolution dispersers, especially by the bluest G140M grating, and the PRISM allows for robust identification of spectral features such as broad and narrow lines in both rest-UV and rest-optical parts of the spectrum.

3.1. Target Selection

In the last year many BL AGN have been successfully identified via their broad band colors and rest-frame optical compactness, and subsequently verified via the presence of broad lines in their rest-optical spectra (Greene et al. 2024; Furtak et al. 2024; Killi et al. 2023; Kocevski et al. 2023; Kokorev et al. 2023a; Wang et al. 2024). Namely, using a combination of broad-band NIR-Cam colors covering the characteristic "break" feature present in LRDs and a compactness criterion was shown to be extremely successful (> 80%) at identifying broad line AGN with photometry and size alone.

To identify our targets we use the same criteria as Labbé et al. (2023a), Greene et al. (2024), and Kokorev et al. (2024), aiming to maintain a consistent approach in selecting LRDs, particularly regarding aperture sizes. These are as follows:

$$\begin{aligned} \text{red}\,\mathbf{1} &= \text{F}115\text{W} - \text{F}150\text{W} < 0.8 &\&\\ &\text{F}200\text{W} - \text{F}277\text{W} > 0.7 &\&\\ &\text{F}200\text{W} - \text{F}356\text{W} > 1.0 \end{aligned}$$

https://archive.stsci.edu/hlsp/jades

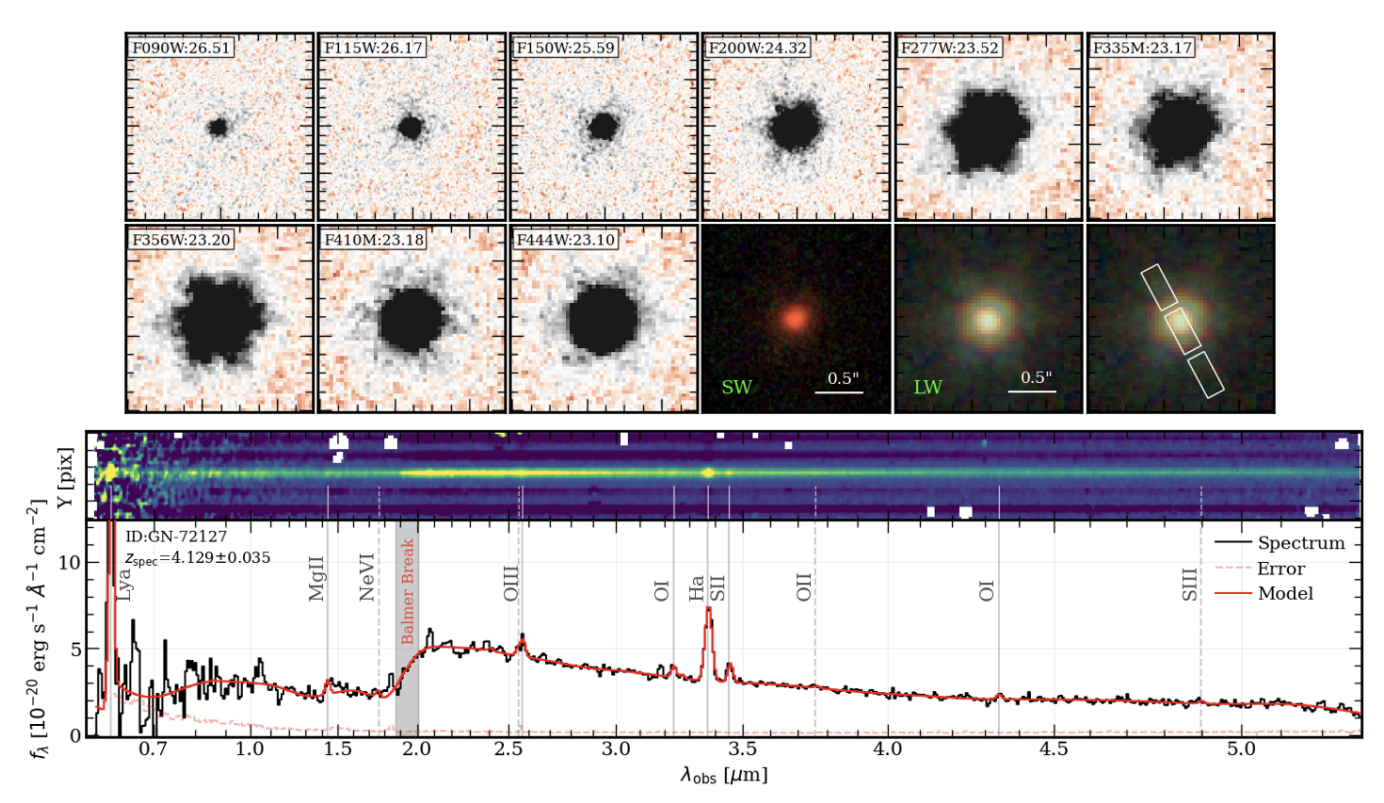


Figure 1. Top: JWST/NIRCam~2''0 stamps and the RGB short and long wavelength color images comprised of the F115W, F150W, F200W and F277W, F356W, and F444W bands, respectively. The MSA slitlet layout (white) is overlaid on a separate LW color image, for clarity. The source has a very clear PSF-dominated morphology present in all filters. Each panel shows the total magnitude as presented in the JADES DR3 catalog (D'Eugenio et al. 2024). The source is extremely bright and is detected in all bands at $> 50\sigma$. Middle: 2D MSA PRISM spectrum. Bottom: Optimally extracted 1D spectrum of the galaxy in the observed frame. We show the data in black, while the uncertainty on the spectrum is in dashed red. Best-fit spline continuum and line MSAEXP model to the data is shown in solid red. Assuming the best-fit to the PRISM with $z_{\rm spec} = 4.129 \pm 0.035$, we show the positions and label the prominent emission with significant ($> 3\sigma$) detections as solid vertical lines. Emission lines for which we only obtain an upper limit are shown with dashed lines. The position of the Balmer/4000 Å break is shown with a shaded region.

or
$$\label{eq:red2} \begin{array}{c} \text{red2} = \text{F150W} - \text{F200W} < 0.8 & \& \\ \text{F277W} - \text{F356W} > 0.6 & \& \\ \text{F277W} - \text{F444W} > 0.7, \end{array}$$

plus the compactness cut given by:

compact =
$$f_{\text{f444w}}(0.4)/f_{\text{f444w}}(0.2) < 1.7$$
.

The final selection is then (red1|red2) & compact.

The JADES GOODS-N DR3 public photometric catalog includes both circular aperture and total (i.e., Kron) photometry for 85,709 sources in the GOODS-N field (D'Eugenio et al. 2024). Since we are focusing on compact sources, we specifically use $D=0^{\prime\prime}3$ apertures (CIRC2) and convert them to total fluxes using the aperture corrections provided by the JADES team. These smaller apertures offer a good balance for reliably measuring fluxes of point-like objects (e.g., see Kokorev et al. 2023a; Kocevski et al. 2024; Labbé et al. 2023a; Trus-

sler et al. 2024), while keeping aperture corrections relatively low. Finally, we also require for the object to be covered by all 3 medium resolution gratings and the PRISM, and also have a valid redshift from the JADES catalog (D'Eugenio et al. 2024).

Using this selection method, we first identify 11 LRDs in the data ranging from $z\sim 4-7$, all targets have clear rest-optical line detections in the PRISM, as well as the G235M and G395M gratings. Moreover, 4/11 LRDs that we find were already confirmed and presented as BL AGN in a work by Maiolino et al. (2023b). Not all however have significant line detections in the rest-UV, covered by the G140M grating and PRISM. This is imperative to our study as we aim to simultaneously examine the rest-UV and rest-optical properties of LRDs. Despite that, we find that a single source from the initial 11 stands out in particular, owed to its broad lines in the rest-optical and multiple line detections in the rest-UV.

Table 1. Source Properties

R.A.	189.265718	
Dec	62.168393	
$z_{ m spec}$ (PRISM)	4.129 ± 0.035	
$z_{\rm spec}~({ m G235M})$	4.1306 ± 0.0004	
$z_{\rm spec}~({ m G395M})$	4.1295 ± 0.0005	
$A_{\rm V}~({\rm H}\alpha/{\rm H}\beta)~[{ m mag}]$	$1.1^{+0.8}_{-0.1}$	
$r_{ m eff,optical} \; [m pc]$	< 300	
$r_{ m eff,UV} \; [m pc]$	490 ± 50	
FWHM [km/s]		
Narrow Lines (G235M, G395M)	510 ± 72	
Broad Lines $(H\alpha)$	2573 ± 585	
Narrow Mg II	482 ± 371	
Broad Mg II	1100 ± 535	
Absorption Lines (Host)	959 ± 162	
$\log_{10}(M_{ m BH}/M_{\odot})~({ m H}lpha)$	7.31 ± 0.21	
$\log_{10}(M_{ m BH}/M_{\odot}) \; (L_{5100})$	7.90 ± 0.15	
$\log_{10}(M_{ m dyn}/M_{\odot})$	< 10.76	
$\log_{10}(\Sigma_*/M_{\odot}{ m kpc}^{-2})$	< 11.01	
$L_{\rm bol} \ [{\rm erg} \ {\rm s}^{-1}]$	$(3.46 \pm 1.10) \times 10^{44}$	
$\mathrm{Ly} \alpha \ \mathrm{EW}_0 \ [\mathrm{\AA}]$	400 ± 50	
BAGPIPES Non-Parametric SFH Fit		
$A_{\rm V}$ (continuum) [mag]	0.43 ± 0.08	
$\log_{10}(M_*/M_{\odot})$	10.63 ± 0.05	
Mass-weighted Age [Gyr]	$0.74^{+0.21}_{-0.29}$	
${ m SFR_{10}} \; [M_{\odot}/{ m yr}]$	$0.036^{+0.818}_{-0.025}$	
${ m SFR}_{100} \left[M_{\odot} / { m yr} ight]$	$0.070^{+0.847}_{-0.047}$	
Z/Z_{\odot}	0.97 ± 0.16	
$\log_{10}(U)$	-3.07 ± 0.13	

We thus identify GN-72127, a potential AGN candidate at z = 4.1288, located at R.A. = $189^{\circ}.265718$, decl.= 62°.168393 (Table 1). Consistent with LRDs selected in previous studies, GN-72127 is red in the restoptical but remains visible, albeit moderately red, in the rest-UV. It is also very bright in the F444W broad-band filter ($\sim 23.1 \text{ mag}$) while remaining completely point-like (see Section 3.9). Of prime interest to our work, however, is the spectral coverage of GN-72127. A combination of NIRSpec/PRISM observations and, most crucially, the exquisite coverage by three medium-resolution dispersers ($t_{\text{int}}=3107 \text{ s each}$) provides the most comprehensive set of data to date for investigating the physics of these reddened AGN. We present 2".0 cutouts of the source in each medium and broad-band NIRCam filter alongside a PRISM spectrum in Figure 1.

Table 2. Measured emission line fluxes † and rest-frame equivalent widths of absorption lines (EW₀)

equivalent widths of absorption lines (EW ₀)		
Line	$\lambda_{\mathrm{rest}} [\mathrm{\mathring{A}}]$	Flux $[10^{-20} \text{ erg s}^{-1} \text{ cm}^{-2}]$
$-$ Ly α	1215.4	2875.8 ± 288.1
Mg II (narrow)	2796.5	122.2 ± 60.0
Mg II (broad)	2796.5	90.1 ± 40.2
Mg II (narrow)	2803.1	142.5 ± 60.5
Mg II (broad)	2803.1	225.8 ± 95.2
[Ne III]	3867.9	123.5 ± 40.5
[O III]	4363.0	108.4 ± 25.5
$H\beta$ (narrow)	4862.7	105.5 ± 55.0
[O III]	4959.5	155.2 ± 32.2
[O III]	5007.2	307.7 ± 35.5
OI	6302.2	169.8 ± 30.5
NII	6549.0	293.0 ± 25.6
$H\alpha$ (narrow)	6562.8	444.0 ± 94.1
$H\alpha$ (broad)	6562.8	742.8 ± 150.0
NII	6585.2	625.7 ± 77.4
Не і	6680.0	72.7 ± 23.2
SII	6716.5	104.9 ± 30.0
SII	6731.8	80.2 ± 25.8
I O	8446.0	53.0 ± 17.5
Absorption Lines		
Line	$\lambda_{\rm rest} [{\rm \AA}]$	EW ₀ [Å]
$\mathrm{H}\eta$	3835.4	7.0 ± 0.6
${ m H}\zeta$	3889.1	6.6 ± 1.0
Ca K	3934.0	1.4 ± 1.1
${ m H}\epsilon$	3970.1	12.0 ± 1.6
${ m H}\delta$	4101.7	4.1 ± 1.9
${ m H}\gamma$	4340.4	5.5 ± 1.5
$H\beta$ (absorption)	4862.7	16.3 ± 4.4
$H\alpha^1$ (absorption)	4862.7	1.41 ± 0.5

 $^{^{\}dagger}$ No dust correction was applied.

Despite clear AGN signatures in LRDs, a vast majority of them remains X-ray undetected (e.g. see Akins et al. 2024; Greene et al. 2024; Maiolino et al. 2024; Pacucci & Narayan 2024). In line with this, we also find nothing at the position of the source in the deep (~ 170.43 ks) Chandra data (Brandt 2001).

3.2. Initial Line Identification

We start our investigation of all available low and medium resolution spectra by running a heavily modified version of MSAEXP (Brammer 2022). Briefly, MSAEXP models emission and absorption lines as Gaus-

¹ Derived from the best-fit BAGPIPES stellar model.

sians and fits the continuum as a series of cubic splines, albeit at a fixed (and user defined) velocity width for all lines. Our key modifications² to the code include making the line width a free parameter, and also adding an option to fit the same line with multiple components (i.e., narrow and broad). For each available spectrum of the source, we allow the fit to search for the best fit within a narrow redshift range ($\Delta z \sim 0.02$), with the prior set by drawing from the JADES spectroscopic catalog. We overlay the best fit to the PRISM in Figure 1.

We find that the $z_{\rm spec}$ derived from the PRISM and 3 medium resolution dispersers match up quite well, without any significant offsets (< 150 km/s). With this approach we identify a number of the key features. These are - a potential broad Mg II and H α emission, strong [O III] and [N II] doublets, a strong Balmer break as well as the higher order (H γ through H η) Balmer absorption features (Figure 2). The latter two imply that the rest-optical continuum could be dominated by an older stellar population. All of the above are securely identified in PRISM as well as the gratings. We also note a very prominent Ly α emission, albeit only in the PRISM, which has insufficient spectral resolution to compute any systemic velocity offset.

We note that not all spectral lines can be modeled well by our routine. While it is adequate at fitting the majority of narrow and broad spectral features rather quickly, which is useful for large samples of spectra, its reliability is quickly diminished by intricacies of certain line complexes. This is especially apparent when uncommon line ratios are required, in the regions where S/N is low or the continuum is simply too noisy. A robust identification of certain spectral features, such as broad lines, is imperative to properly classify the object. Therefore, we will focus on certain parts of the spectrum with a more sophisticated procedure, which we will describe in subsequent sections.

3.3. G395M: Broad $H\alpha + /NII$

Compared to the PRISM the G395M grating has a much higher spectral resolution which allows us to resolve the, otherwise blended, emission from the [N II] doublet and $H\alpha$. The [S II] doublet remains blended however. Crucially, the availability of multiple spectral pixels sampling the line complex enables us to try and fit both broad and narrow components to the Balmer emission. While we do not detect any contaminant lines in the spectrum we note the presence of corrupted data (NaN values) in the spectrum, likely a result of issues during data reduction or 1D spectrum extraction. These

features are, however, minor and do not affect our fitting routine. In addition, as we already mentioned in Section 2, due to the MSA configuration employed by the JADES team, the spectra can overlap, resulting in additional lines from neighboring sources. However, as the redshift for the source is known precisely, these contaminant lines are easily masked out.

We fit each line complex simultaneously alongside the continuum. Each emission line is modeled with a standard Gaussian profile, with the position allowed to vary within a narrow redshift range around the bestfit MSAEXP solution. We fix the ratio between the $[N_{II_{\lambda6549}}]$ and $[N_{II_{\lambda6585}}]$ to 1:3, respectively, as is normally done in the literature (e.g. see de Graaff et al. 2024). We also fit the H α emission with both narrow and broad components. The ratio between lines in the [SII] doublet is allowed to vary freely. All narrow line velocities are tied together and we assume the same redshift for all lines. Finally, we model the local continuum with a first order polynomial. Given the limited number of spectral pixels we do not include an absorption component when we fit the $H\alpha$, as the fit would become too degenerate. Instead, to account for $H\alpha$ absorption, we use the best-fit stellar continuum model fitted to the host galaxy as described in Section 3.8. The derived line fluxes of H α and [N II] lines are then corrected for the stellar absorption. Generally however, the EW of the stellar absorption is comparable for all Balmer lines, meaning that the redder (i.e. $H\alpha$) absorption lines have a weaker contribution to the spectra, compared to the higher order lines, and are thus less important to take into account.

The fit is initialized by creating all of the models on an oversampled grid, which is then interpolated onto the wavelength axis that mimics the heterogeneous grating resolution. Finally, we allow for a custom over sampled spectral resolution scaled by a factor of 1.3. It was shown that a spectral resolution of a point-like source can be higher than that of a source uniformly illuminating the slitlet (see e.g. de Graaff et al. 2023; Greene et al. 2024; Kokorev et al. 2023a). The best fit is a found via a nonlinear least-squares minimization, with the MCMC uncertainty derived from the covariance matrix.

From the fit we derive a redshift of $z_{\rm spec} = 4.1294 \pm 0.004$, FWHM of the narrow lines (H\$\alpha\$, [N II], [S II]) equal to 510 ± 72 km/s and a broad H\$\alpha\$ component with a width of 2573 ± 585 km/s. We strongly detect the [N II] and [S II] doublets, and recover both narrow and broad H\$\alpha\$ components at 3σ level. To verify whether a broad line fit is required at all, we perform additional modeling without allowing for a broad H\$\alpha\$ emission. To verify the significance of this broad-line we calculate the Bayesian

² A modified code is available upon request.

Information Criterion (BIC) difference between the narrow+broad and narrow lines-only fits. We find the narrow only fit to be an inadequate representation of the data (BIC_{narrow}-BIC_{narrow+broad}= Δ BIC> 20), which indicates a very strong evidence (using the criteria defined in Jeffreys 1961) for the broad component being present in H α .

We measure $\log_{10}([N \text{ II}]_{\lambda 6586}/\text{H}\alpha)=0.15^{+0.24}_{-0.16}$, which is too high to have originated from star-formation (Kewley et al. 2001; Grossi et al. 2009). The [SII] doublet at $\lambda\lambda6717,6731$ Å is another useful diagnostic for gas ionization when coupled with the adjacent $H\alpha$ line. We also find it to be elevated, with $\log_{10}([S \text{ II}]_{\lambda\lambda6717,6731}]/\text{H}\alpha) = -0.38^{+0.21}_{-0.13}$. While it is possible to reach these high line ratios via e.g. shocks, the presence of a robust broad H α emission exceeding 2000 km/s, much faster than could be explained by shocks (Allen et al. 2008), gives us the first hint as to the presence of an AGN (Kewley et al. 2006) in this otherwise seemingly stellar-light dominated galaxy. The best-fit is presented in the rightmost panel of Figure 2. For now we will refrain from making a definitive statement regarding the AGN presence and will explore other gratings.

3.4. G235M: $H\beta$ and OIII

We continue our investigation by shifting to a bluer medium resolution disperser - G235M (middle panel of Figure 2). Following the same fitting procedure as before, we now fit the H β line with two components (emission and absorption), and the [O III] where we do not fix the ratio between the lines. We assume the same velocity dispersion for all emission lines and leave the velocity of the absorption line to be independent. The H β is fit with only a single narrow component.

Firstly, we derive a $z_{\rm spec} = 4.1307 \pm 0.005$, consistent with the G395M, FWHM of the emission lines equal to 529±81 km/s and a largely unconstrained broad absorption component with a width of 2429 ± 835 km/s. We strongly detect the narrow [O III] doublet and find the FWHM to match that of the narrow lines in the G395M grating. Therefore it is likely that $H\alpha$, $H\beta$, [NII], [OIII]and [SII] originate from the same region in the galaxy. We also confirm a very weak $H\beta$ emission, marginally detected at $\sim 1.5\sigma$ level. At the same time we also can clearly detect an $H\beta$ line in absorption, however the noise present around that feature does not allow us to securely identify the width of that feature. While uncertain, what is clear is that the absorption profile is wider compared to the emission lines. We will focus on all available absorption features and their widths in the next sections. Notably, while the narrow H β is largely undetected we can still use this information and derive the lower limit on the $\log_{10}([O\,\text{III}]_{\lambda 5007}/H\beta) > 0.50$. This high value again puts us at odds with having originated purely from star formation.

3.5. G140M: MgII

Finally we focus on the last available grating the G140M. As is typical of LRDs, the object is rather faint in the rest-UV as such we do not detect a large array of lines in this disperser compared to the other ones, however one feature stands out. We perform a fit to the Mg II doublet ($\lambda\lambda 2796, 2803$) with a narrow and broad component for each, as shown in the left panel of Figure 2. During the fit we allow the Mg II 2796/Mg II 2803 ratio to vary freely. We find the FWHM of the narrow component to be equal to 482 ± 371 km/s, not constrained as well as for the other narrow lines in the spectrum, but still consistent within the uncertainty. Including the broad component, we find its width to be equal to 1100 ± 535 km/s, marginally detected at $\sim 2\sigma$ level. As before we attempt the same fit with a narrow only Mg II doublet, and find it to be moderately worse ($\Delta BIC=2.5$), compared to the narrow+broad fit. We also find that the Mg II 2796/Mg II 2803 for both narrow and broad lines is consistent with the accepted ranges $\sim 0.5-1$ within the uncertainty (Laor et al. 1997; Wang et al. 2009).

While the evidence is not as strong as for the broad $H\alpha$, we will refrain from making a definitive statement on whether the broad Mg II emission is present in the rest-UV spectrum of the source. This possibility however can not be ruled out either, as it does appear that a broad-line component makes the fit better. The potential presence of broad Mg II emission provides us with another piece of the evidence that an active black hole might be present in GN-72127.

Just like the broad hydrogen features, broad Mg II lines are also formed in the BLR, but typically originate slightly farther out from the central black hole compared to e.g. H α . This difference in location can result in somewhat lower velocities for Mg II-emitting gas clouds (see e.g. Wang et al. 2009), which is what we find in our fit. In addition, the S/N of the G140M at the position of Mg II barely allows us to model the continuum, as such broader Mg II wings are obscured by the noise, making our derived line width lower than what it is in reality.

3.6. Balmer Decrement

It is well established that the ratio between observed fluxes of Balmer series lines can be used to determine the dust extinction. Given the quiescent nature of the source we have a strong reason to believe that all observed emission lines originate from either the NLR or the BLR around an AGN. As such applying the dust at-

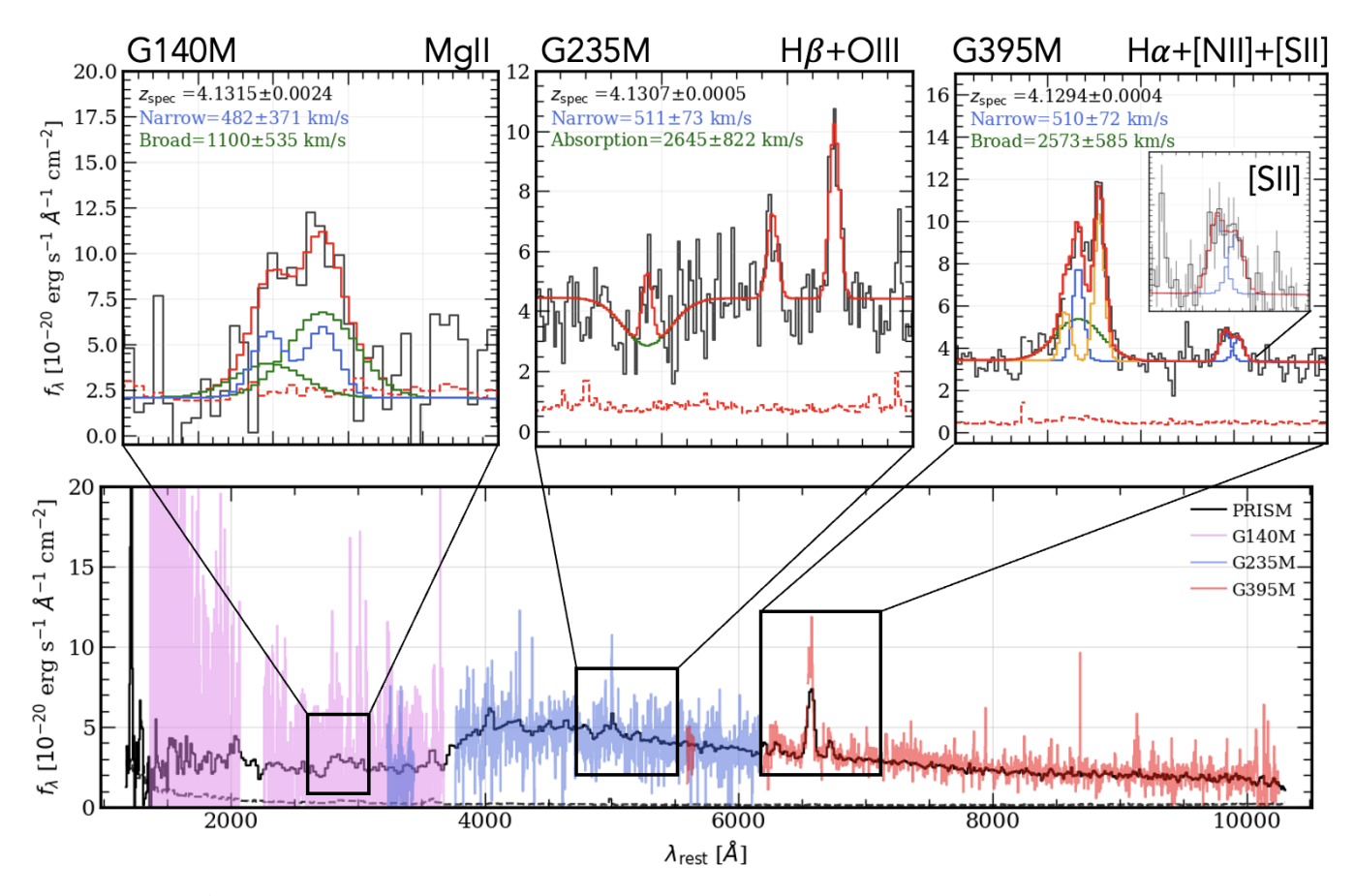


Figure 2. Top: A series of panels showing fits to the main line series of interest. From left to right these are, a tentative broad line fit to the Mg II doublet; H β and [O III] doublet; H α , [N II] and [S II] doublets. We show best-fit narrow lines in blue, apart from the [N II] which is shown in orange for clarity. The broad emission (or absorption) best fits are shown in green. The total combined model including the continuum is plotted in red. The original spectrum is in black and the error spectrum is dashed red. **Bottom:** Full collection of all available medium and low resolution MSA spectra. These are as follows, PRISM (black), G140M (violet), G235M (blue) and G395M (red). The presence of broad lines in the G140M and G395M spectra is our first hint of AGN activity.

tenuation derived from the continuum would not be adequate to derive AGN properties. To compute the $A_{\rm V}$ we use the narrow line ratio - ${\rm H}\alpha/{\rm H}\beta$ computed from our fits to the G395M and G235M dispersers. As mentioned in Section 3.4, the narrow ${\rm H}\beta$ line is only detected at 2σ , so our $A_{\rm V}$ would only be an approximation. By doing this we find ${\rm H}\alpha/{\rm H}\beta\approx 4.28$. Provided the same ratio holds between narrow and broad emission lines, we also confirm that the broad component in ${\rm H}\beta$ would not be detectable in our data (EW₀ ~ 5 Å), thus justifying our narrow only fit to ${\rm H}\beta$ in Section 3.4.

In line with other works on reddened quasars (e.g. see Hopkins et al. 2004), high-z galaxies (Capak et al. 2015; Reddy et al. 2015, 2018), and LRDs themselves (e.g. Furtak et al. 2024; Greene et al. 2024; Kokorev et al. 2023a) we use the Small Magelannic Cloud (SMC) reddening law (Gordon et al. 2003). Assuming that case

B recombination applies in the NLR of an AGN (Osterbrock 1989), we find that the observed line ratio gives us a moderate attenuation of the region around the central black hole equal to $A_{\rm V}=1.1^{+0.8}_{-0.1}$.

3.7. Other Notable Lines

Beyond the lines discussed in earlier sections, the spectra reveal a multitude of other emission and absorption features. As these are quite numerous, considering the volume of data for this object alone, we will not focus on each one individually, but rather point out some that could be of particular interest to our study. The derived fluxes for all lines in our work can be found in Table 2.

We fit the Ly α emission in the PRISM spectrum using a single Gaussian model, allowing both the FWHM and redshift to vary. Due to a limited spectral resolution of the PRISM at this wavelength ($R \sim 60$), we are un-

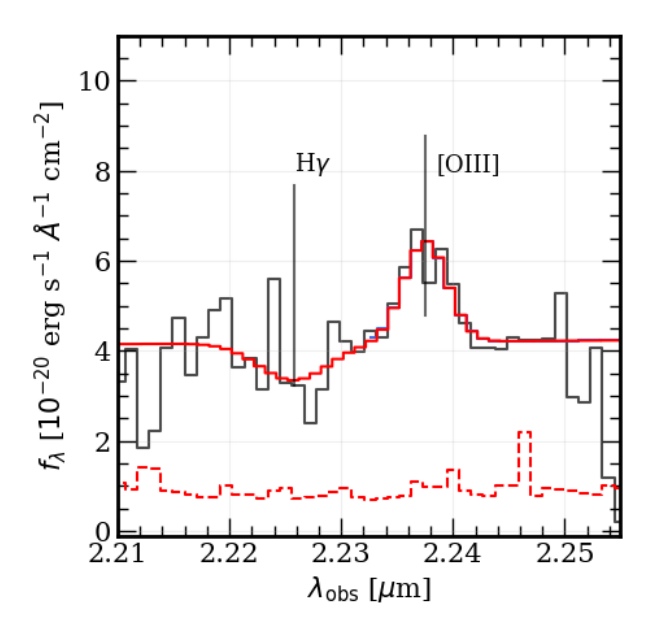


Figure 3. A fit to the H γ and $[O\,\textsc{iii}]\lambda4363$ lines. The spectrum is in black and the total fit is in red. The error spectrum is shown in dashed red. The velocity widths and redshift were fixed to the values form the previous fits. The derived intrinsic $[O\,\textsc{iii}]\lambda4363/[O\,\textsc{iii}]\lambda5007$ of ~ 0.5 is indicative of extremely high ionization, likely induced by AGN activity.

able to precisely measure the width or offset of this line from the systematic redshift. However, the line spans 3 spectral pixels, each approximately 900 km/s wide in the rest frame, suggesting that the Ly α emission in GN-72127 could be broad. Notably, the line is quite strong, with a measured rest-frame equivalent width (EW₀) of 400 ± 50 Å, significantly exceeding the typical values found in star-forming galaxies at $z \sim 4.5$ (Zheng et al. 2014; Hashimoto et al. 2017).

In the G235M spectrum we identify the auroral [O III] $\lambda 4363$ line, which can be used to trace both ionization and metallicity. It has been suggested that at higher metallicities [O III] can blended with the adjacent [Fe III] $\lambda 4360$ line (e.g. see Curti et al. 2017). We attempt two fits, one including the [Fe III] line and one without it. In both cases we fix the velocity widths and redshift to the other narrow lines. Our results indicate that the [O III] line by itself better represents the data, as opposed to fitting it alongside [Fe III] ($\Delta BIC \sim 3$). Given that there are only so many spectral pixels covering the line, we believe that the fit with a $\lambda 4360$ feature line is simply too degenerate to yield an adequate BIC. Therefore, we cannot entirely rule out the possibility that $[O III]\lambda 4363$ is free from contamination. This is well reflected in our uncertainties on the derived line flux. We show the best fit to the line in Figure 3.

Finally, we note the presence of the O I $\lambda 8446$ line detected in the PRISM spectrum at $\sim 3\sigma$ significance Table 2. The O I line is produced through the Ly β fluorescence process which involves the absorption of Ly β photons by neutral oxygen, which is then re-emitted at 8466 Å. This process requires dense, highly ionized environments, such as the BLR of an AGN (Osterbrock & Ferland 2006).

3.8. Exploring the Host Galaxy

So far we have identified broad line emission, enhanced emission line ratios and a high $\mathrm{Ly}\alpha$ EW which all point toward a presence of an AGN in GN-72127. Despite that, the unambiguous presence of the Balmer break and associated absorption lines in the spectrum clearly indicates that the majority of the continuum emission in GN-72127 is still likely dominated by older stars. To this end we would like to perform a dedicated fit to the host galaxy in order to derive the properties of the stellar population in GN-72127.

The available JWST PRISM and medium grating data are jointly fit with the BAGPIPES SED fitting code (Carnall et al. 2018, 2019). The setup for the fit is as follows. We adopt a non-parametric SFH with the 'bursty continuity' prior from Tacchella et al. (2022), using eight time bins where the SFR is fit to a constant value in each bin. The first four bins are set to lookback times of 0-3 Myr, 3-10 Myr, 10-30 Myr, and 30-100 Myr, while the last four bins are logarithmically spaced between 100 Myr and $t_{\text{max}} = t_{\text{universe}}(z = z_{\text{spec}}) - t_{\text{universe}}(z = 20)$. Dust attenuation is assumed to follow the Calzetti et al. (2000) law and the rest-frame V-band attenuation is fit (log-uniform prior) in the range $A_{\rm V} = 0.001 - 5$ mag. Stellar nebular emission is included with an ionization parameter in the range $-4 \le \log U \le -2$. We allow for a stellar velocity dispersion in the range 50–500 km/s and metallicity between 0.1–2.5 Z_{\odot} (log-uniform prior for both). Finally, we allow BAGPIPES to modify the input spectral noise array by a factor between 0.5-2. As mentioned above, the AGN-like ratios of the narrow emission lines imply that they potentially originate in the NLR, rather than the host. We therefore have removed the contribution of the emission lines to our fit by masking them out.

From the BAGPIPES fit we find the galaxy to be very massive $\log_{10}(M_*) = 10.63 \pm 0.02$, with little dust attenuation $(A_{\rm V} \sim 0.4)$ and essentially devoid of all star-formation activity $(\log_{10}({\rm sSFR}) < -11.5)$. The best-fit SFH reveals a short burst of star-formation some ~ 300 Myr ago, which lasted for ~ 100 Myr, forming at roughly 40-60 $M_{\odot}/{\rm yr}$. The galaxy then appears to have quenched rapidly at $z \sim 5.5$, remaining largely

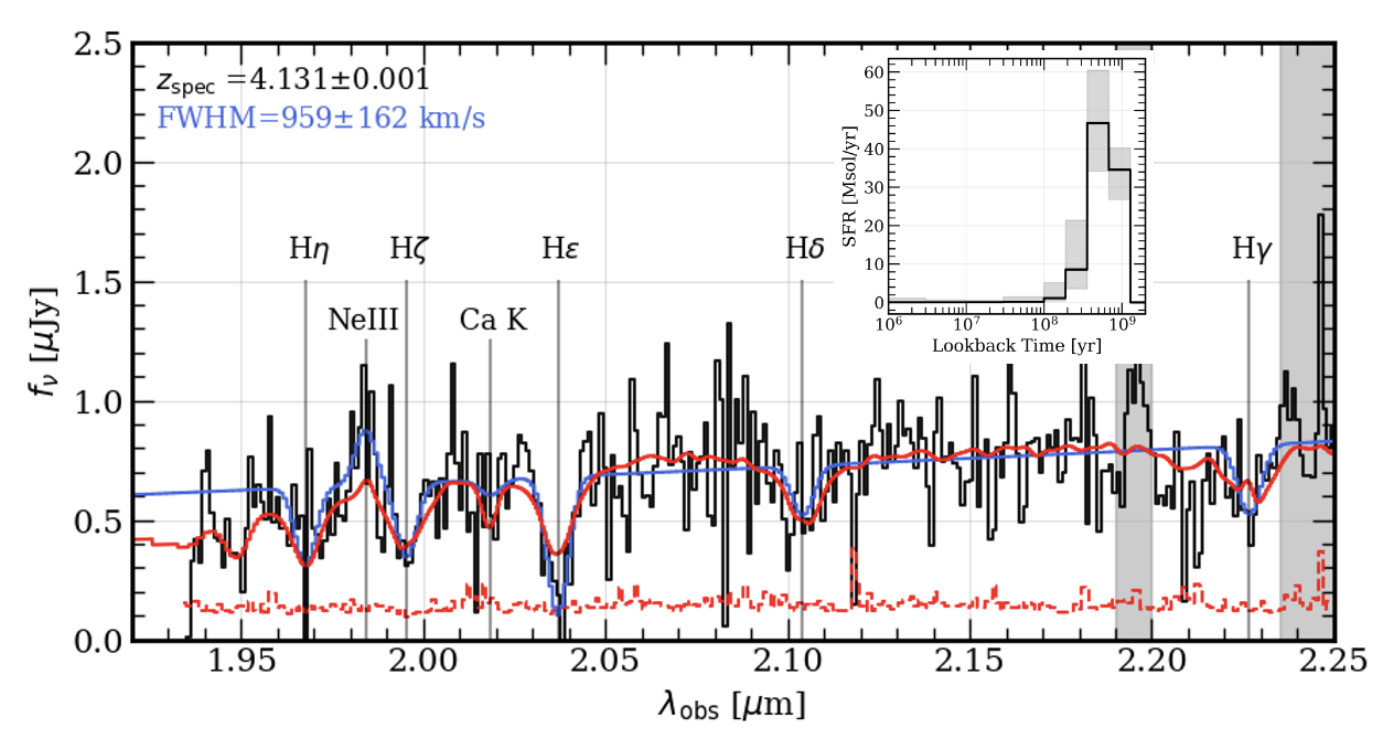


Figure 4. Examination of the absorption features in the G235M spectrum of the quiescent host galaxy. We show our best fit to the absorption lines+[Ne III] in blue, while the non-parametric SFH BAGPIPES fit is in red. The regions of the spectrum (black) that were masked out due to contaminant lines are shown as a shaded area. The error array is in dashed red. This galaxy exhibits deep Balmer absorption lines with the spectrum resembling that of an A-type star, common in lower-redshift post-starburst galaxies (Goto 2007; Wild et al. 2009, 2020), as well as most recent exploration of z > 4 quiescent galaxies (Carnall et al. 2023; de Graaff et al. 2024). On the inset we show the best-fit non-parametric SFH, which clearly shows that GN-72127 experienced a significant, rapid drop in the SFR within the last $\sim 200 - 300$ Myr ($z \sim 5.8$).

dormant all the way until the time we observed it. In Figure 4 we present the best-fit BAGPIPES SED, along-side a line-specific fit to the relevant part of the spectrum containing absorption lines. An array of high order Balmer absorption lines from $\rm H\eta$ to $\rm H\gamma$, alongside a tentative detection of the Ca K feature is reminiscent of the highest-z quiescent galaxies found with $\it JWST$ (Carnall et al. 2023; de Graaff et al. 2024).

While BAGPIPES measures the width of the absorption features alongside other parameters, that fit was done on data that span multiple spectral resolutions, thus the derived widths might be inadvertently broadened. To keep all of our velocity measurements consistent, we have re-fit all of the absorption features, as well as the Ne III emission with the same method as in Section 3.3. We show our final result in Figure 4. For the absorption lines we derive a FWHM of 959 ± 162 km/s. This corresponds to the velocity of the stars in the galaxy, rather than the gas, as was done in previous works concerning BL AGN (Maiolino et al. 2023b). The absorption lines from stars trace the dynamical mass, and are broader than the narrow lines (FWHM/2.355 = $\sigma_* = 407 \pm 71$ km/s), consistent with the notion that all

our narrow emission lines likely originate from the NLR, rather than the host galaxy.

3.9. Size Measurements

As the cutouts in Figure 1 indicate, the source is very compact, bordering on unresolved in the redder bands. We now would like to measure the effective radius ($r_{\rm eff}$) to confirm whether that is indeed the case by modeling the object with GALFIT (Peng et al. 2002, 2010). When fitting we take into account the effects of the PSF, which we have measured empirically from the bright stars in the field. We model the object with a Sérsic (Sérsic 1963) profile where the source position, brightness, effective radius, Sérsic index, and axis ratio as allowed to vary.

In all LW bands (F277W, F356W, F410M, F444W) the measured effective radius varies from $0\rlap.{''}034-0\rlap.{''}04$. In this case a source can be considered to be point-like and unresolved since its effective radius is smaller than the empirical PSF HWHM ($\sim0\rlap.{''}07$ for F444W). It is however possible to measure sizes of objects that are smaller that the PSF as shown was shown by other works on compact objects (van der Wel et al. 2014; Labbé et al.

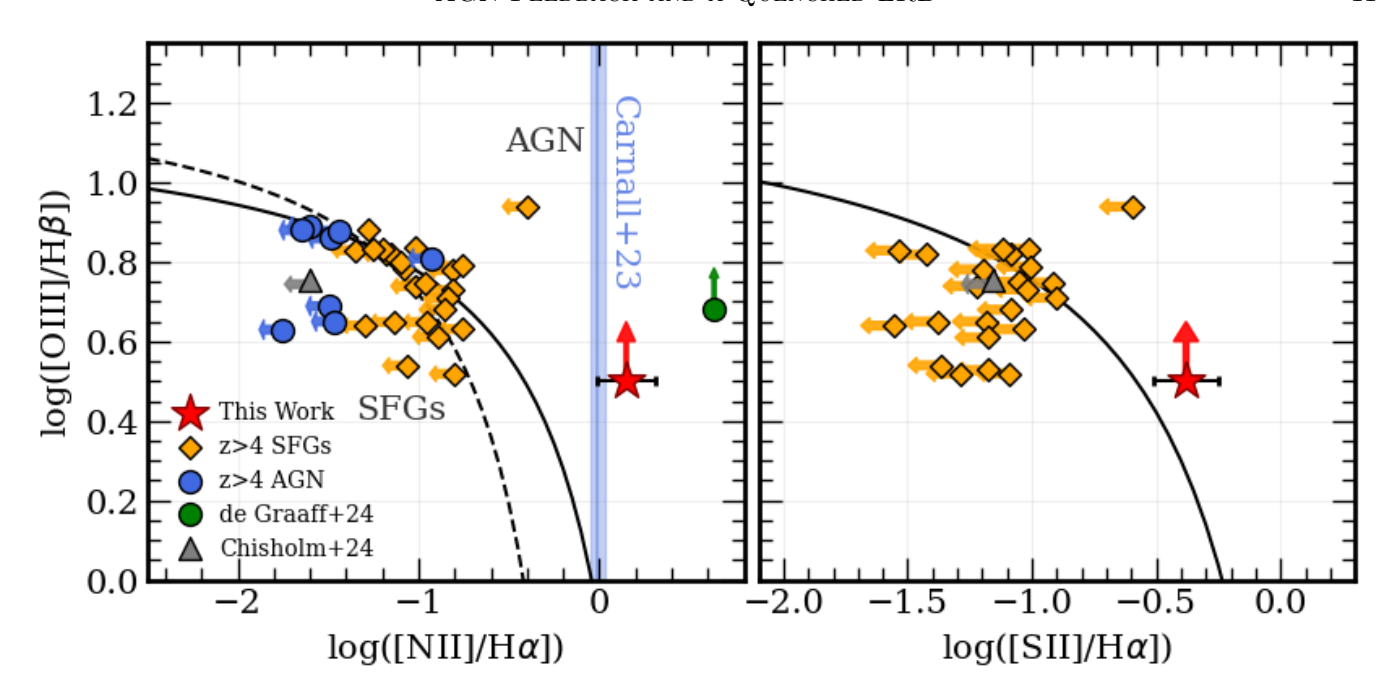


Figure 5. BPT (left) and BPT-[S II] (right) ionization diagnostics. The [N II] and [S II] to Hα line ratios found in the object (red) appear to vastly exceed those found in high-z SFGs (orange; Cameron et al. 2023; Sanders et al. 2023), Type I (blue; Maiolino et al. 2023b) and Type II AGN (grey; Chisholm et al. 2024). On the other hand we find a comparable ionization to the highest-z QG from de Graaff et al. (2024) (green) and Carnall et al. (2023) (vertical blue line). The line ratios we find are indicative of AGN-dominated ionization as the tracks from Kewley et al. (2001) (solid) and Kauffmann et al. (2003) (dashed) appear to suggest.

2023a). Taking the redshift into account, we derive an upper limit on the physical effective radius to be $\lesssim 300$ pc. The point-like nature and size of this source in restoptical is consistent with a highly concentrated, PSF dominated objects explored in the recent exploration of high-z reddened AGN (Furtak et al. 2024; Kocevski et al. 2024; Kokorev et al. 2023a, 2024; Labbé et al. 2023a) as well as the similarly compact highest-z quiescent galaxies (Carnall et al. 2023; de Graaff et al. 2024).

On the other hand, we marginally resolve the source in the rest-UV, sampled by all other bluer filters, with the median size across all SW filters equal to $0.07 \pm 0.07 \pm 0.01$, roughly $\times 2.5$ larger than the PSF (HWHM $\sim 0''.025$), resulting in $r_{\rm eff} = 490 \pm 50$ pc. We also derive a Sérsic index $n \approx 1.15$, implying a lower degree of central concentration in the rest-UV. As GN-72127 is not resolved in rest-optical it is difficult to say with a high degree of certainty if GN-72127 has a more compact morphology in the redder filters. Although it is entirely feasible that the extended emission present in the rest-UV might imply that this part of the spectrum is dominated by stars, rather than the AGN light. A similar finding has already been reported in a stellar-light dominated LRD with extremely strong Balmer emission (Labbé et al., in prep.).

Next, we would like to use the effective radius to gauge the dynamical mass as well as the stellar surface density (Σ_*) . As the stellar light will be dominant at longer, rest-optical wavelengths, this would make the F444W band the most physically constraining for this type of study, as was done in Labbé et al. (2023a). The F444W band should also trace the region with the lowest amount of dust obscuration.

Using the derived velocity widths of the absorption lines and the F444W size of the object we derive the dynamical stellar mass by following $M_{\rm dyn} = 5 r_{\rm eff} \times \sigma_*^2/G$, where G is the gravitational constant, (Cappellari et al. 2006; de Graaff et al. 2024). The σ we derive in Section 3.8 is explicitly that of the stellar population itself, and should better trace the true M_* (plus gas and dark matter) as opposed to the widths of narrow nebular lines. Given the $r_{\rm eff} < 300$ pc and the stellar velocity dispersion – $\sigma_* = 407 \pm 71 \text{ km s}^{-1}$ – we obtain an upper limit on $M_{\rm dyn} < 10.76~M_{\odot},$ fully consistent with the M_* we measure from SED fitting. Finally, we derive an upper limit on the stellar mass surface of $\log_{10}(\Sigma_*/M_{\odot} \text{kpc}^{-2}) < 11.01$. This is high but does not exceed the maximum limits attainable during an intense burst of star formation (Hopkins et al. 2010; Grudić et al. 2019), and is consistent with some of the densest

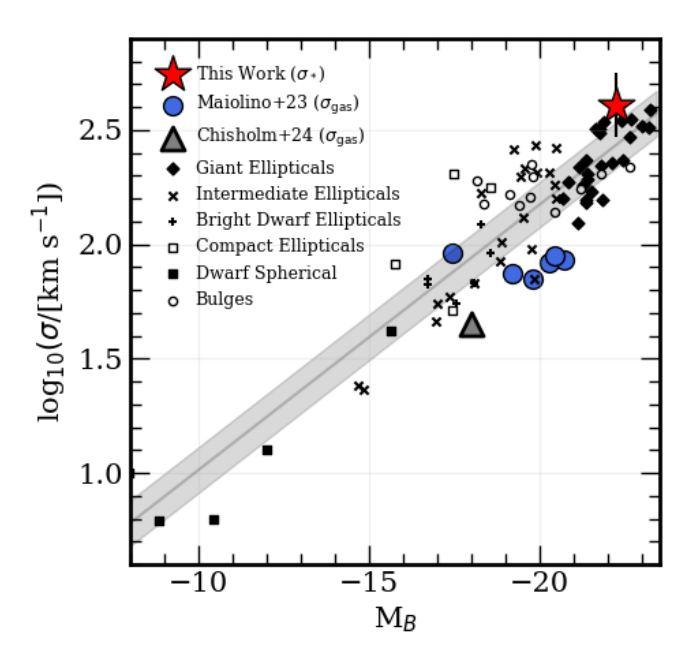


Figure 6. An exploration of $z\sim 4-7$ AGN on the fundamental Faber-Jackson relation (solid line; Faber & Jackson 1976; Shen et al. 2008; Cappellari 2016). We show GN-72127 in red, Type I AGN from Maiolino et al. (2023b) in blue, and Type II AGN from (Chisholm et al. 2024) in grey. For comparison we additionally overlay results for various local elliptical, spherical and bulge galaxies (Bender et al. 1992). The source is located exactly on the Faber-Jackson relation, signifying how it is already similar to local ellipticals at $z\sim 4$, and further implying that the continuum is indeed stellar dominated.

recently discovered quiescent galaxies at high-z (Carnall et al. 2023; de Graaff et al. 2024).

4. RESULTS

4.1. Black Hole Properties

Time domain observations of local guasars draw a correlation between the width of the broad Balmer series lines and the size of the BLR (e.g., Kaspi et al. 2000; Greene & Ho 2005), allowing for the BH mass to be estimated from the width of the emission lines and their luminosities. We compute the BH mass $(M_{\rm BH})$ from the luminosity and the width of the broad H α line, and restframe 5100 Å luminosity of the underlying continuum. Since we have established that the Balmer emission most likely all comes from the region around the AGN itself, i.e. the narrow and broad line regions (NLR and BLR), we will use the $A_{\rm V}$ value derived from the Balmer decrement, and assume that NLR and BLR have similar amounts of dust extinction, to correct the $H\alpha$. On the other hand, the rest-optical continuum is likely to be stellar light dominated, so we will use an $A_{\rm V} \sim 0.4$ value derived from the BAGPIPES fit (rather than $A_{\rm V}\sim 1.1$ from the decrement) to the host galaxy when correcting the L_{5100} .

With the above considerations in mind, from the $H\alpha$ we derive $\log_{10}(M_{\rm BH,H\alpha}/M_{\odot})=7.31\pm0.21$ and from the continuum we get $\log_{10}(M_{\rm BH,5100}/M_{\odot}) = 7.90 \pm 0.15$. The uncertainty on both of these estimates is largely dominated by the scatter in the relations used to derive the masses, rather than the errors on the line flux and/or dust extinction (Kollmeier et al. 2006). If the rest-optical was mostly dominated by the AGN emission, one would expect both of these results to be consistent (e.g. see Kokorev et al. 2023a), however we find that the 5100 Å estimate, even with a comparably modest dust obscuration, returns a mass that is $\times 5$ higher. This in return might imply that despite the $H\alpha$ line being clearly detectable, the continuum around it is still dominated by the stellar light. The degree to which this is happening is highly uncertain, and would require dedicated modeling of the continuum to determine the fractional contribution of the AGN light to the total SED, which is made difficult by the lack of data redder of the F444W band. As such, for the rest of this work we will adopt the $M_{\rm BH}$ derived from the H α luminosity as our final result.

In addition to the mass, we also use the broad ${\rm H}\alpha$ to derive the bolometric luminosity ($L_{\rm bol}$) of the AGN. We use $L_{\rm bol}=130\times L_{\rm H}\alpha$ (Richards et al. 2006; Stern & Laor 2012) and obtain $L_{\rm bol}=(3.46\pm1.10)\times10^{44}$ erg/s. Using the above values, the $L_{\rm bol}/L_{\rm edd}$ is then ≈ 0.12 , implying that the object is accreting at a sub-Eddington rate. This is much lower compared to the extreme AGN found at high-z (Furtak et al. 2024; Larson et al. 2023; Kokorev et al. 2023a; Maiolino et al. 2023b), however some AGN at high-z also appear to be less active (Kocevski et al. 2023; Matthee et al. 2023) or even completely dormant (Juodžbalis et al. 2024).

4.2. Ionization

As briefly stated in the previous sections, some of the nebular narrow lines ratios in the source look elevated when compared to massive star-forming galaxies. In this section we would like to explore this further and investigate the potential ionization mechanisms in the galaxy.

In Figure 5 we show the $[O\,\textsc{iii}]/H\beta$ ratio as a function of $[N\,\textsc{ii}]/H\alpha$ and $[S\,\textsc{ii}]/H\alpha$. Given a strong absorption feature present in $H\beta$ (Figure 2) we only report these ratios as upper limits. Both $[N\,\textsc{ii}]$ and $[S\,\textsc{ii}]$ doublets are however detected at S/N>3 (Table 2) and should provide a more robust diagnostic. Our derived line ratios place us securely in the AGN locus of the BPT (Baldwin et al. 1981) diagram, with regions delimited by Kewley

et al. (2001) and Kauffmann et al. (2003). In addition we also derive $\log_{10}([{\rm OI}]\lambda6302/{\rm H}\alpha) \sim -0.42$, which again securely places us in the AGN portion of the ionization diagnostic (Kewley et al. 2006).

We also observe an extremely high ratio between the auroral $[O III]\lambda 4363$ line and $[O III]\lambda 5007$ (RO3) of $0.35_{-0.15}^{+0.17}$, and $0.54_{-0.25}^{+0.35}$ when applying the NLR dust correction we derive in Section 3.6, respectively. This is quite extreme, and does exceed the dust-corrected RO3=0.32 found in $z \sim 8.5$ LRD by Kokorev et al. (2023a). The object also appears to be highly ionized when compared to high-z SFGs, with RO3=0.048 presented by (Katz et al. 2023). Even if our dust-correction is overly aggressive, the observed ratio we find is hard to reconcile with ranges laid out in Nicholls et al. (2020) and will lead to extreme electron temperatures and densities. However, photoionization models presented in Baskin & Laor (2005) alongside RO3 studies from decades of low-z Seyfert investigations (Koski & Osterbrock 1976; Osterbrock 1978; Ferland & Netzer 1983; Dopita & Sutherland 1995; Nagao et al. 2001; Binette et al. 2022, just to name a few) do imply that the necessary high temperatures and densities can be reached in the NLR around an AGN. As mentioned in the previous section, high metallicities can cause the [Fe III] $\lambda 4360$ line to contaminate the $[O III]\lambda 4363$ flux (Curti et al. 2017). Although our fit to the spectrum does not show evidence of [Fe III] emission, the NLR can be easily enriched with metals due to its relatively low mass, resulting in the contribution of this line to $[O III]\lambda 4363$ to be potentially non-negligible. This could mean that our RO3 is overestimated, but only higher resolution data from the Hgratings can be used to definitely answer this question. Another possibility for such a high ratio is a highly dense NLR. The critical density of $[O III]\lambda 4363$ is roughly $50 \times$ higher than that of $[O III]\lambda 5007$, so if the density of some regions within the NLR exceeds 10^{5.8} cm⁻³, then RO3 can be artificially boosted as well.

4.3. AGN Quenching in a Little Red Dot

With all the pieces in place, we now would like to examine the full picture and reflect on the potential nature of the source. While GN-72127 fulfills color and compactness criteria for LRDs, the colors themselves seem to originate from the evolved stellar population, rather than AGN continuum. All signs point toward GN-72127 being a massive ($\log_{10}(M_*) \sim 10.6$) quiescent galaxy. The SFH inferred from a multitude of absorption lines as well as a strong Balmer break indicate that this galaxy has ceased, at least temporarily, its star formation. In the rest-optical, a combination of broad lines and AGN-like line ratios, betrays a moder-

ately active AGN $(L_{\rm bol}/L_{\rm edd} \sim 0.1)$ with a black hole mass of $\log_{10}(M_{\rm BH}) \sim 7.3$, embedded within this massive, quenched galaxy. At the same time, in the rest-UV we detect a strong (EW ~ 400 Å) Ly α , inconsistent with the low SFR of the host, plus a Mg II doublet in emission. While the evidence for the broad component in Mg II is itself tentative, the mere fact that we find this line in emission in a solar metallicity quiescent galaxy, already strongly suggests it originates from an AGN and not star formation (Burchett et al. 2021; Witstok et al. 2021).

While the LRD we study has clear AGN signatures, such as broad lines and AGN-like ionization, it does appear to have completely settled on the local relations linking black holes and their host galaxies. For example, we find the $M_{\rm BH}/M_*$ in GN-72127 to be completely consistent with the local relations (Kormendy & Ho 2013; Greene et al. 2016, 2020). While the narrow lines in the source likely originate from the NLR around an AGN, the availability of clear stellar absorption features allows us to robustly measure the stellar velocity dispersion. We place GN-72127 on the Faber-Jackson sequence (Faber & Jackson 1976) in Figure 6 and find that the object has largely "settled" onto the same evolutionary trajectory as local elliptical galaxies that exist on the fundamental plane (Djorgovski & Davis 1987). This is unsurprising as we find that the source does in fact have a lot in common with the massive quiescent galaxies recently uncovered by JWST (Carnall et al. 2023; de Graaff et al. 2024), rather than the record breaking high-z LRDs. In the final section we would like to reflect on how this source potentially came to be, and where it might be headed.

5. DISCUSSION AND SUMMARY

5.1. Recently Discovered AGN and Their Hosts

The last two years of observations with JWST have provided us with constraints on $M_{\rm BH}/M_*$ for a large sample of AGN across a wide epoch of early cosmic history (z=4-9). We aim to explore these data to determine if there is an evolutionary link between AGN-dominated high-z objects with high $M_{\rm BH}/M_*$ (Bogdan et al. 2023; Endsley et al. 2023; Goulding et al. 2023; Kokorev et al. 2023a; Juodžbalis et al. 2024), reddened AGNs at $z\sim 4$ which have grown their stellar populations significantly over the last $\lesssim 1$ Gyr (Labbé et al., in prep, Wang et al. 2024), and the earliest quiescent galaxies at z>4 (Carnall et al. 2023; de Graaff et al. 2024).

In Figure 7, we show how the $M_{\rm BH}/M_*$ relation evolves for JWST-detected AGN and quiescent galaxies containing AGN signatures, compared to the local

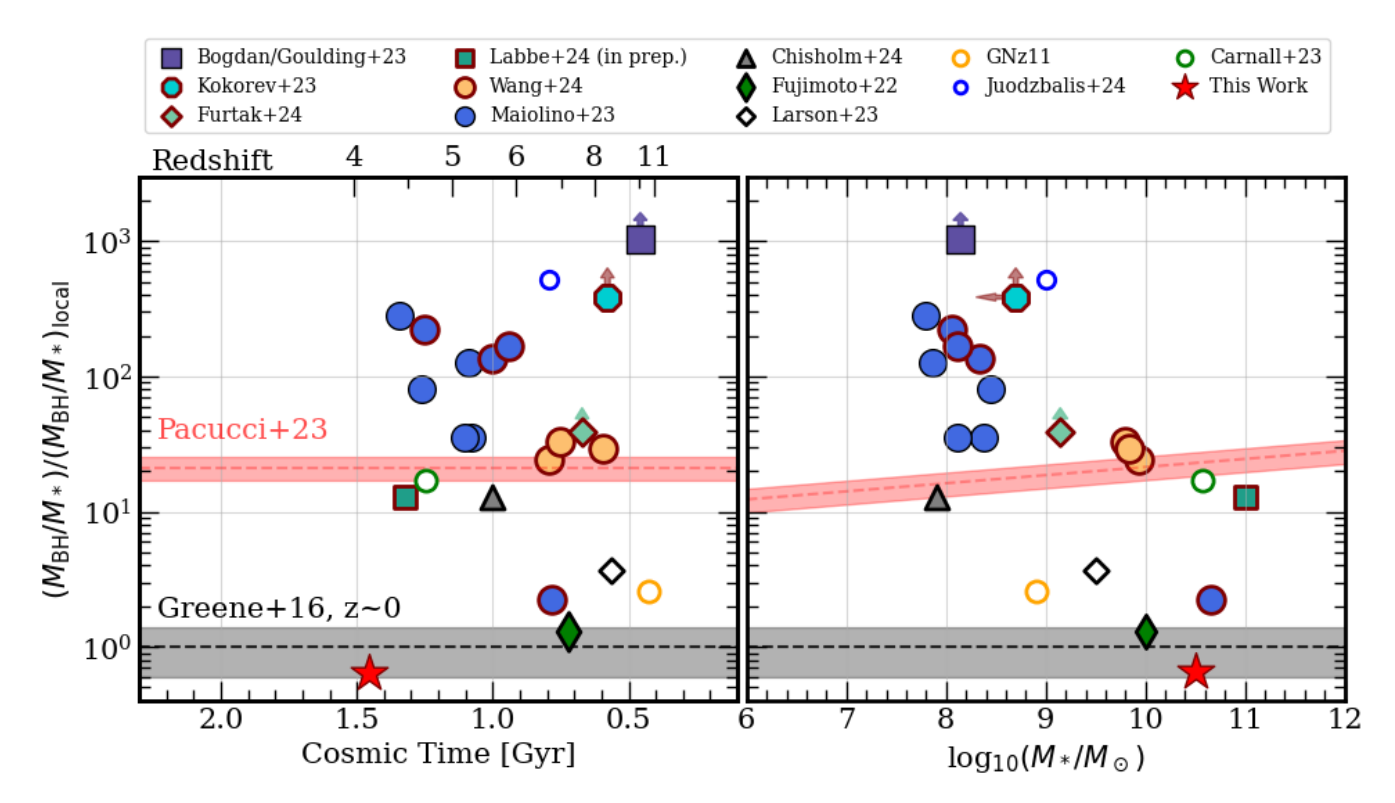


Figure 7. Potential evolution of the offset between derived $M_{\rm BH}/M_*$ and a local relation (Greene et al. 2024) across time (left) and stellar mass (right). We show an array of high-z AGN (Bogdan et al. 2023; Goulding et al. 2023; Chisholm et al. 2024; Fujimoto et al. 2022; Furtak et al. 2024; Juodžbalis et al. 2024; Kokorev et al. 2023a; Larson et al. 2023; Maiolino et al. 2023a,b; Wang et al. 2024). We specifically highlight objects that would be selected as LRDs with a red envelope. In gray and maroon we also show tracks of $M_{\rm BH}/M_*$ relations from Greene et al. (2024) and Pacucci et al. (2023), respectively. We note the emergent downward trend of $M_{\rm BH}/M_*$ toward the local relations.

relation (Greene et al. 2024), as a function of both cosmic age (redshift) and stellar mass. Starting with the epoch just ~ 400 Myr ($z \sim 11$) after the Big Bang, we cover roughly 1 Gyr of cosmic history in order to reflect on a potential evolutionary path that can tie this picture together.

Formation mechanisms of AGN with elevated $M_{\rm BH}/M_{*}$ ratios remain elusive. Proposed solutions range from super-Eddington accretion on remnants of Population III stars (Furtak et al. 2024; Larson et al. 2023) and compact starbursts (Kroupa et al. 2020), to direct collapse seeds (Bogdan et al. 2023; Daval et al. 2024; Goulding et al. 2023; Kokorev et al. 2023a; Natarajan et al. 2023; Maiolino et al. 2023b) and primordial black holes (Liu & Bromm 2022; Dayal 2024). These overmassive black holes could also be explained by by the existence of a new $M_{\rm BH}-M_{*}$ sequence (Pacucci et al. 2023; Pacucci & Loeb 2024), or a high covering fraction, implying that locally-calibrated virial relations which link black hole mass to $H\alpha$ luminosity are not applicable at high-z (Maiolino et al. 2024; Pacucci & Narayan 2024). The perceived excess of these highmass BHs could also simply stem from a selection bias in luminosity-limited BL samples where the outliers are the only detectable sources and a change to the underlying scaling relations is not necessary (Li et al. 2024). Formation pathway aside, AGN with very little to no detectable host galaxy component have been found across a multitude of extragalactic fields, too many to be ignored.

While the gas in these systems might not be fueling star formation, a considerable amount is still required to sustain AGN accretion. In their work Maiolino et al. (2023b) present a sample of high-z AGN (45% being LRDs, using the same criteria as in Section 3.1) which do not follow the local $M_{\rm BH}-M_*$ relation but align with local dynamical black hole mass relations. This would imply that these systems do contain gas but are inefficient at forming stars. The initial view of the farinfrared (FIR) emission in LRDs provided by ALMA reveals a dearth of SF activity, albeit these observations still remain relatively shallow. So far, not a single LRD has been detected in the FIR (Akins et al. 2024; Casey et al. 2024; Labbé et al. 2023a). It has even been sug-

gested that most LRDs are not AGN, but rather compact starburst galaxies instead (Pérez-González et al. 2024a; Williams et al. 2023), as they lack a rising power-law in the mid-infrared (MIR). There is no evidence so far from the MIR/FIR to support or refute that notion, and objects with clear AGN signatures have been found to also show a lack of a dusty torus emission (Wang et al. 2024), which could be a result of a patchy BLR (Maiolino et al. 2024).

At lower redshifts ($z \sim 4-5$), we are presented with another curiosity: some objects that fulfill the LRD criteria (Labbé et al. 2023a; Greene et al. 2024) also appear to contain evolved stellar populations. Model fits to these systems indicate very early and rapid star formation, followed by a significant reduction (Wang et al. 2024; Labbé et al., in prep.) or near cessation of SF activity, as in GN-72127, as they approach the local $M_{\rm BH}-M_*$ relation. This source, in particular, provides a unique opportunity to examine the $M_{\rm BH}-M_*$ ratio and the SFH in reddened AGN with unprecedented detail. The clearly stellar-dominated continuum and broad H α emission allow us to extract information concerning both the central black hole and detailed properties of the stellar population in the host galaxy.

Contrasting the SFH of GN-72127, with the objects in Wang et al. (2024), reveals a scenario where compact, reddened AGN enter a starburst phase 300 - 400Myr before the epoch of observation and then appear to quench. This indicates that there is a stage between elevated and local-like $M_{\rm BH}-M_*$ where these AGN experience rapid star formation, possibly due to a shutdown of AGN feedback, gas virialization, a merger, or a combination of multiple factors. During this stage, we expect that these AGN would be still identifiable (e.g. through high ionization or broad lines), but would also shine brightly in the FIR as they are now actively (and rapidly) forming stars. Given that this phase is shortlived (~ 100 Myr), catching these objects in the act is challenging, although it may have already been accomplished.

In their pre-JWST work, Fujimoto et al. (2022) presented GNz7q, a compact object at $z \sim 7.2$, which potentially bridges quasars at cosmic dawn with galaxies at cosmic noon. The spectral shape and extremely high UV-luminosity surface density of GNz7q indicate it cannot be explained by extreme star formation alone, suggesting its AGN nature. At the same time it is embedded in an extremely FIR luminous host starburst galaxy (SFR_{IR} > 1600 M_{\odot}/yr), all within ~ 480 pc, precisely the type of transitioning, short-lived object we were looking for. Moreover, GNz7q is extremely faint in X-rays, suggesting a Compton-thick, super-Eddington

black hole accretion disk, a characteristic observed in high-z AGN (Endsley et al. 2023; Furtak et al. 2024; Greene et al. 2024; Kokorev et al. 2023a; Maiolino et al. 2023a). It does appear that star-formation can take place in galaxies hosting massive AGN and can do so at quite an accelerated rate. Notably, GNz7q is a very extreme example but there likely exists a small population of LRD hosts in the starburst phase, that is yet to be identified. It is very possible that these are NIRCam dark, due to extreme dust obscuration $(A_{\rm V} > 4-5)$ and low surface brightness, making the detection of rest-UV/optical emission extremely challenging. The existence of such dusty systems at high redshift was briefly explored in Kokorev et al. (2023b), and recently, a NIRCam-dark source was identified by Pérez-González et al. (2024b), yet the exact number densities of these objects are still unclear.

5.2. Evolution and Link to the Quiescent Galaxies

A multitude of studies preceding the launch of JWST have laid out the possibility that cores of the most massive galaxies in our local Universe have, in fact, formed very rapidly. This is generally thought to happen via a burst of star-formation at z>5-6, followed by a rapid quenching (Thomas et al. 2005; Conroy et al. 2014; van Dokkum et al. 2015).

The identification and detailed analysis of z=3-5 quiescent galaxies, made possible with NIRSpec, have further supported the notion of rapid star-formation and subsequent quenching (Carnall et al. 2023; de Graaff et al. 2024; Glazebrook et al. 2024). Some of these galaxies seemingly retain their AGN signatures as either broad lines (Carnall et al. 2023) or high ionization (de Graaff et al. 2024). The sample presented recently in Wang et al. (2024) seems to show the progenitors of some of these quiescent galaxies as their star-formation undergo a truncation. The authors propose a scenario where massive galaxies have simultaneously grown alongside their SMBHs and then proceed to quench rapidly, however we would like to offer an alternative interpretation.

It is possible that the systems with elevated $M_{\rm BH}/M_*$ we find with JWST will undergo episodes of intense star formation. These are likely induced through merging, as many LRDs were found to exist in overdensities (Fujimoto et al. 2023; Greene et al. 2024; Kokorev et al. 2023a; Labbé et al., in prep.). Following a short-lived yet intense starburst, like the one observed in Fujimoto et al. (2022) or predicted by Carnall et al. (2023) and de Graaff et al. (2024), the stellar mass of the host galaxy catches up to its over-massive BH and settles onto the local BH-host relations. The next likely step of their

evolution is further expansion and transition toward the giant ellipticals we see locally.

Having undergone a burst and then a rapid quenching (Figure 4), GN-72127 appears to agree with this picture. Dominated by stellar light the object still contains clear AGN signatures, which suggests that rapid quenching could have been driven by AGN feedback rather than gas depletion. We propose that while some high-z AGN may not initially follow concurrent growth of BHs and their stellar populations, they will eventually "settle" onto the local relations, as time progresses.

Generally, elliptical galaxies are thought to form through processes such as mergers of smaller galaxies. During these mergers, the system undergoes violent relaxation, redistributing energy and leading to a state of equilibrium. The duration of such a process will be longer for extended and less massive systems, and shorter for the most massive and compact ones. We can see how close the source is to a "settled" virialized state by examining its position on the Faber-Jackson relation Figure 6. We find that GN-72127 occupies a position very similar to the local ellipticals, implying that such virialization may already take place quite early, at $z \sim 4$, potentially for the most massive objects. On the other hand BHs with measured σ from Maiolino et al. (2023b), especially the ones with similar stellar mass, are at higher redshift compared to GN-72127 and are likely still evolving into their equilibrium state. The achievement of a virial equilibrium is crucial to our argument, as then it would make it difficult for galaxies to have significant $M_{\rm BH}/M_*$ variations as their stellar masses exceed $\sim 10^{10} \text{ M}_{\odot}$, ultimately aligning them with local relations.

Despite this, we find that our source is offset from the local $M_{\rm BH} - \sigma$ relation (e.g. Kormendy & Ho 2013; Greene et al. 2020). Our derived σ_* suggests a $M_{\rm BH} \sim$ $10^9 M_{\odot}$, ~ 2 dex higher than our current measurement. It is therefore possible that the stellar component of GN-72127 still requires more time to relax and expand from its very compact configuration to align with the local $M_{\rm BH} - \sigma$ trend, due to the conservation of angular momentum, driving down the σ . Importantly, we do not observe any compact objects with LRD colors below $z \sim 4$ (Kocevski et al. 2024), supporting the idea that these objects have begun to expand and dynamically relax into structures resembling lower-z ellipticals. Furthermore, studies of elliptical galaxies from z=2 to 0 show that their effective radii grow by a factor of 2-4over ~ 10 Gyr timescales (van der Wel et al. 2008; Cassata et al. 2011; van der Wel et al. 2014; Xie et al. 2015). This observed growth and relaxation process is consistent with the transformation of LRDs into the quiescent elliptical galaxies we see at lower redshifts.

It is worth noting that objects presented in Figure 7 do not necessarily follow these exact evolutionary paths. A large fraction of high-z AGN have poorly measured M_* as the AGN continuum dominates the emission making it difficult to separate the two (see discussion in Greene et al. 2024; Wang et al. 2024). Dynamical masses can be employed instead, however the same problem manifests itself when trying to decide whether the narrow nebular lines originate from the NLR or the host galaxy itself. In the case of GN-72127, however, the stellar-dominated continuum and the presence of absorption lines allows for robust measurements of both M_* and $M_{\rm dyn}$.

5.3. Final Remarks

Using the NIRSpec PRISM and medium resolution G140M, G235M, G395M observations of the GOODS-N field (D'Eugenio et al. 2024), we present the investigation of a little red dot that shows signs of both an evolved stellar population and AGN activity at z = 4.13. A careful examination of the spectrum of the source shows a significant (> 4σ) BL component present in the H α line with a FWHM of ~ 2500 km/s. As we do not observe similar broad features in the strongly detected [NII], [SII] or the [OIII] lines, we suggest that the broadening exhibited by $H\alpha$ is a sign of an actively accreting black hole, rather than large-scale outflows. A further evidence for the AGN activity are high ionization inferred from the BPT diagram, the RO3 line diagnostic, as well as a strong Ly α emission with an EW₀ ~ 400 Å. In the rest-UV we also report a tentative broad component in the Mg II doublet, which could further strengthen our AGN interpretation.

Despite being compact and showing clear AGN signatures, GN-72127 appears to be different from the high-z LRDs explored with NIRSpec (Furtak et al. 2024; Kokorev et al. 2023a; Greene et al. 2024). We detect a massive ($\log_{10}(M_*) \sim 10.6$) and evolved host, which dominates the continuum of our object, as evidenced by a strong Balmer break as well as a multitude of absorption lines. Detailed SFH fitting reveals that our object has formed most of its stellar population in a short (100-200 Myr) burst, and then quenched rapidly roughly 200 Myr ago. It is worth noting that stellar masses of LRDs are generally poorly constrained due to difficulties separating the AGN and stellar continuum. Despite that, a strong stellar that we detect in GN-72127 would be clearly visible even at high-z, provided it was there.

We contrast the position of GN-72127 on the $M_{\rm BH}/M_*$ vs z and M_* plane to all other high-z LRDs and BL AGN uncovered with JWST. This examination

reveals a potential evolutionary path that starts with overmassive BH in the early Universe, which then form stars in a rapid burst and slowly descend onto the local $M_{\rm BH}-M_*$ relation occupied by local ellipticals.

Finally, we detect very strong Ly α emission, inconsistent to have come solely from star formation, and a tentative broad line in Mg II doublet. This would mean that, for the first time, we now see clear AGN signatures in the rest-UV spectra of LRDs. Despite that we can not yet ascertain the full origins of blue light in LRDs. While we detect emission lines with strong AGN signatures in the rest-UV, we also find it to be marginally resolved $(\sim 500 \text{ pc})$, too large to have come just from the central AGN alone. It is likely that some AGN light indeed escaped the thick dust cover through either scattering and some patchy coverage, but the continuum itself is likely to be stellar in origin. Rest-UV emission in GN-72127 appears to originate both from stars and AGN, however this still might not be true for the entire population, especially as we move to higher redshifts where AGN seem to be much more dominant. Although it is worth noting still, that observational bias can drive the high incidence of objects with elevated $M_{\rm BH}/M_{*}$ (e.g. Li et al. 2024). Only dedicated deep studies of the rest-UV emission of LRDs with medium and high resolution NIRSpec gratings onboard JWST can shine more light on this mystery.

ACKNOWLEDGMENTS

VK acknowledges support from the University of Texas at Austin Cosmic Frontier Center. We thank the JADES team for providing the scientific community with these beautiful JWST data. This work is based on observations made with the NASA/ESA/CSA James Webb Space Telescope. The data were obtained from the Mikulski Archive for Space Telescopes at the Space Telescope Science Institute, which is operated by the Association of Universities for Research in Astronomy, Inc., under NASA contract NAS 5-03127 for JWST. Some of the data products presented herein were retrieved from the Dawn JWST Archive (DJA). DJA is an initiative of the Cosmic Dawn Center, which is funded by the Danish National Research Foundation under grant No. 140. The X-ray datasets were obtained from the Chandra Xray Center.

Software: BAGPIPES (Carnall et al. 2018, 2019), EAZY (Brammer et al. 2008), grizli (Brammer 2023), msaexp (Brammer 2022).

Facilities: JWST

REFERENCES

Akins, H. B., Casey, C. M., Allen, N., et al. 2023, ApJ, 956, 61, doi: 10.3847/1538-4357/acef21

Akins, H. B., Casey, C. M., Lambrides, E., et al. 2024, arXiv e-prints, arXiv:2406.10341,

doi: 10.48550/arXiv.2406.10341

Allen, M. G., Groves, B. A., Dopita, M. A., Sutherland, R. S., & Kewley, L. J. 2008, ApJS, 178, 20, doi: 10.1086/589652

Baldwin, J. A., Phillips, M. M., & Terlevich, R. 1981, PASP, 93, 5, doi: 10.1086/130766

Barro, G., Perez-Gonzalez, P. G., Kocevski, D. D., et al. 2023, arXiv e-prints, arXiv:2305.14418, doi: 10.48550/arXiv.2305.14418

Baskin, A., & Laor, A. 2005, MNRAS, 358, 1043, doi: 10.1111/j.1365-2966.2005.08841.x

Bender, R., Burstein, D., & Faber, S. M. 1992, ApJ, 399, 462, doi: 10.1086/171940

Binette, L., Villar Martín, M., Magris C., G., et al. 2022, RMxAA, 58, 133,

doi: 10.22201/ia.01851101p.2022.58.01.11

Bogdan, A., Goulding, A., Natarajan, P., et al. 2023, arXiv e-prints, arXiv:2305.15458,

doi: 10.48550/arXiv.2305.15458

Brammer, G. 2022, msaexp: NIRSpec analysis tools, 0.3, doi: 10.5281/zenodo.7299500

Brammer, G. 2023, grizli, 1.8.2, Zenodo, Zenodo, doi: 10.5281/zenodo.7712834

Brammer, G. B., van Dokkum, P. G., & Coppi, P. 2008, ApJ, 686, 1503, doi: 10.1086/591786

Brandt, W. 2001, The Chandra Survey of the Hubble Deep Field North Area: a Public Resource for the Present and Future of X-Ray Astronomy, Chandra Proposal ID 03900164

Bunker, A. J., Saxena, A., Cameron, A. J., et al. 2023, A&A, 677, A88, doi: 10.1051/0004-6361/202346159

Burchett, J. N., Rubin, K. H. R., Prochaska, J. X., et al. 2021, ApJ, 909, 151, doi: 10.3847/1538-4357/abd4e0

Calzetti, D., Armus, L., Bohlin, R. C., et al. 2000, ApJ, 533, 682, doi: 10.1086/308692

Cameron, A. J., Katz, H., Rey, M. P., & Saxena, A. 2023, MNRAS, 523, 3516, doi: 10.1093/mnras/stad1579

- Capak, P. L., Carilli, C., Jones, G., et al. 2015, Nature, 522, 455, doi: 10.1038/nature14500
- Cappellari, M. 2016, ARA&A, 54, 597, doi: 10.1146/annurev-astro-082214-122432
- Cappellari, M., Bacon, R., Bureau, M., et al. 2006, MNRAS, 366, 1126, doi: 10.1111/j.1365-2966.2005.09981.x
- Carnall, A. C., McLure, R. J., Dunlop, J. S., & Davé, R. 2018, MNRAS, 480, 4379, doi: 10.1093/mnras/sty2169
- Carnall, A. C., McLure, R. J., Dunlop, J. S., et al. 2019, MNRAS, 490, 417, doi: 10.1093/mnras/stz2544
- —. 2023, Nature, 619, 716, doi: 10.1038/s41586-023-06158-6
- Casey, C. M., Akins, H. B., Kokorev, V., et al. 2024, arXiv e-prints, arXiv:2407.05094.
 - $\rm https://arxiv.org/abs/2407.05094$
- Cassata, P., Giavalisco, M., Guo, Y., et al. 2011, ApJ, 743, 96, doi: 10.1088/0004-637X/743/1/96
- Chabrier, G. 2003, PASP, 115, 763, doi: 10.1086/376392
- Chisholm, J., Berg, D. A., Endsley, R., et al. 2024, arXiv e-prints, arXiv:2402.18643,
 - doi: 10.48550/arXiv.2402.18643
- Conroy, C., Graves, G. J., & van Dokkum, P. G. 2014, ApJ, 780, 33, doi: 10.1088/0004-637X/780/1/33
- Curti, M., Cresci, G., Mannucci, F., et al. 2017, MNRAS, 465, 1384, doi: 10.1093/mnras/stw2766
- Dayal, P. 2024, arXiv e-prints, arXiv:2407.07162. https://arxiv.org/abs/2407.07162
- Dayal, P., Volonteri, M., Greene, J. E., et al. 2024, arXiv e-prints, arXiv:2401.11242. https://arxiv.org/abs/2401.11242
- de Graaff, A., Rix, H.-W., Carniani, S., et al. 2023, arXiv e-prints, arXiv:2308.09742, doi: 10.48550/arXiv.2308.09742
- de Graaff, A., Setton, D. J., Brammer, G., et al. 2024, arXiv e-prints, arXiv:2404.05683, doi: 10.48550/arXiv.2404.05683
- D'Eugenio, F., Cameron, A. J., Scholtz, J., et al. 2024, arXiv e-prints, arXiv:2404.06531, doi: 10.48550/arXiv.2404.06531
- $\label{eq:Diorgovski} \begin{array}{l} \text{Djorgovski, S., \& Davis, M. 1987, ApJ, 313, 59,} \\ \text{doi: } 10.1086/164948 \end{array}$
- Dopita, M. A., & Sutherland, R. S. 1995, ApJ, 455, 468, doi: 10.1086/176596
- Eisenstein, D. J., Willott, C., Alberts, S., et al. 2023a, arXiv e-prints, arXiv:2306.02465, doi: 10.48550/arXiv.2306.02465
- Eisenstein, D. J., Johnson, B. D., Robertson, B., et al. 2023b, arXiv e-prints, arXiv:2310.12340, doi: 10.48550/arXiv.2310.12340

- Endsley, R., Stark, D. P., Lyu, J., et al. 2023, MNRAS, 520, 4609, doi: 10.1093/mnras/stad266
- Faber, S. M., & Jackson, R. E. 1976, ApJ, 204, 668, doi: 10.1086/154215
- Ferland, G. J., & Netzer, H. 1983, ApJ, 264, 105, doi: 10.1086/160577
- Fujimoto, S., Brammer, G. B., Watson, D., et al. 2022, Nature, 604, 261, doi: 10.1038/s41586-022-04454-1
- Fujimoto, S., Wang, B., Weaver, J., et al. 2023, arXiv e-prints, arXiv:2308.11609, doi: 10.48550/arXiv.2308.11609
- Furtak, L. J., Zitrin, A., Weaver, J. R., et al. 2023, MNRAS, 523, 4568, doi: 10.1093/mnras/stad1627
- Furtak, L. J., Labbé, I., Zitrin, A., et al. 2024, Nature, 628, 57, doi: 10.1038/s41586-024-07184-8
- Giavalisco, M., Ferguson, H. C., Koekemoer, A. M., et al. 2004, ApJL, 600, L93, doi: 10.1086/379232
- Glazebrook, K., Nanayakkara, T., Schreiber, C., et al. 2024, Nature, 628, 277, doi: 10.1038/s41586-024-07191-9
- Gordon, K. D., Clayton, G. C., Misselt, K. A., Landolt, A. U., & Wolff, M. J. 2003, ApJ, 594, 279, doi: 10.1086/376774
- Goto, T. 2007, MNRAS, 381, 187, doi: 10.1111/j.1365-2966.2007.12227.x
- Goulding, A. D., Greene, J. E., Setton, D. J., et al. 2023, arXiv e-prints, arXiv:2308.02750, doi: 10.48550/arXiv.2308.02750
- Greene, J. E., & Ho, L. C. 2005, ApJ, 630, 122, doi: 10.1086/431897
- Greene, J. E., Strader, J., & Ho, L. C. 2020, ARA&A, 58, 257, doi: 10.1146/annurev-astro-032620-021835
- Greene, J. E., Seth, A., Kim, M., et al. 2016, ApJL, 826, L32, doi: 10.3847/2041-8205/826/2/L32
- Greene, J. E., Labbe, I., Goulding, A. D., et al. 2024, ApJ, 964, 39, doi: 10.3847/1538-4357/ad1e5f
- Grossi, M., di Serego Alighieri, S., Giovanardi, C., et al. 2009, A&A, 498, 407, doi: 10.1051/0004-6361/200810823
- Grudić, M. Y., Hopkins, P. F., Quataert, E., & Murray, N. 2019, MNRAS, 483, 5548, doi: 10.1093/mnras/sty3386
- Harikane, Y., Zhang, Y., Nakajima, K., et al. 2023, arXiv e-prints, arXiv:2303.11946, doi: 10.48550/arXiv.2303.11946
- Hashimoto, T., Garel, T., Guiderdoni, B., et al. 2017, A&A, 608, A10, doi: 10.1051/0004-6361/201731579
- Heckman, T. M., & Best, P. N. 2014, ARA&A, 52, 589, doi: 10.1146/annurev-astro-081913-035722
- Hopkins, P. F., Murray, N., Quataert, E., & Thompson,T. A. 2010, MNRAS, 401, L19,doi: 10.1111/j.1745-3933.2009.00777.x

- Hopkins, P. F., Strauss, M. A., Hall, P. B., et al. 2004, AJ, 128, 1112, doi: 10.1086/423291
- Iani, E., Rinaldi, P., Caputi, K. I., et al. 2024, arXiv e-prints, arXiv:2406.18207, doi: 10.48550/arXiv.2406.18207
- Jeffreys, H. 1961, Theory of Probability (Oxford, England: (3rd edn.; Oxford Univ. Press))
- Jeon, J., Bromm, V., Liu, B., & Finkelstein, S. L. 2024, arXiv e-prints, arXiv:2402.18773, doi: 10.48550/arXiv.2402.18773
- Juodžbalis, I., Maiolino, R., Baker, W. M., et al. 2024, arXiv e-prints, arXiv:2403.03872, doi: 10.48550/arXiv.2403.03872
- Kaspi, S., Smith, P. S., Netzer, H., et al. 2000, ApJ, 533, 631, doi: 10.1086/308704
- Katz, H., Saxena, A., Cameron, A. J., et al. 2023, MNRAS, 518, 592, doi: 10.1093/mnras/stac2657
- Kauffmann, G., Heckman, T. M., Tremonti, C., et al. 2003, MNRAS, 346, 1055,
 - doi: 10.1111/j.1365-2966.2003.07154.x
- Kewley, L. J., Dopita, M. A., Sutherland, R. S., Heisler,C. A., & Trevena, J. 2001, ApJ, 556, 121,doi: 10.1086/321545
- Kewley, L. J., Groves, B., Kauffmann, G., & Heckman, T. 2006, MNRAS, 372, 961, doi: 10.1111/j.1365-2966.2006.10859.x
- Killi, M., Watson, D., Brammer, G., et al. 2023, arXiv e-prints, arXiv:2312.03065, doi: 10.48550/arXiv.2312.03065
- Kocevski, D. D., Onoue, M., Inayoshi, K., et al. 2023, arXiv e-prints, arXiv:2302.00012, doi: 10.48550/arXiv.2302.00012
- Kocevski, D. D., Finkelstein, S. L., Barro, G., et al. 2024, arXiv e-prints, arXiv:2404.03576, doi: 10.48550/arXiv.2404.03576
- Kokorev, V., Fujimoto, S., Labbe, I., et al. 2023a, ApJL, 957, L7, doi: 10.3847/2041-8213/ad037a
- Kokorev, V., Jin, S., Magdis, G. E., et al. 2023b, ApJL, 945, L25, doi: 10.3847/2041-8213/acbd9d
- Kokorev, V., Caputi, K. I., Greene, J. E., et al. 2024, ApJ, 968, 38, doi: 10.3847/1538-4357/ad4265
- Kollmeier, J. A., Onken, C. A., Kochanek, C. S., et al. 2006, ApJ, 648, 128, doi: 10.1086/505646
- Kormendy, J., & Ho, L. C. 2013, ARA&A, 51, 511, doi: 10.1146/annurev-astro-082708-101811
- Kormendy, J., Bender, R., Magorrian, J., et al. 1997, ApJL, 482, L139, doi: 10.1086/310720
- Koski, A. T., & Osterbrock, D. E. 1976, ApJL, 203, L49, doi: 10.1086/182017

- Kroupa, P., Subr, L., Jerabkova, T., & Wang, L. 2020, MNRAS, 498, 5652, doi: 10.1093/mnras/staa2276
- Labbé, I., Greene, J. E., Bezanson, R., et al. 2023a, arXiv e-prints, arXiv:2306.07320, doi: 10.48550/arXiv.2306.07320
- Labbé, I., van Dokkum, P., Nelson, E., et al. 2023b, Nature, 616, 266, doi: 10.1038/s41586-023-05786-2
- Laor, A., Jannuzi, B. T., Green, R. F., & Boroson, T. A. 1997, ApJ, 489, 656, doi: 10.1086/304816
- Larson, R. L., Finkelstein, S. L., Kocevski, D. D., et al. 2023, arXiv e-prints, arXiv:2303.08918, doi: 10.48550/arXiv.2303.08918
- Li, J., Silverman, J. D., Shen, Y., et al. 2024, arXiv e-prints, arXiv:2403.00074, doi: 10.48550/arXiv.2403.00074
- Liu, B., & Bromm, V. 2022, ApJL, 937, L30, doi: 10.3847/2041-8213/ac927f
- Maiolino, R., Scholtz, J., Witstok, J., et al. 2023a, arXiv e-prints, arXiv:2305.12492, doi: 10.48550/arXiv.2305.12492
- Maiolino, R., Scholtz, J., Curtis-Lake, E., et al. 2023b, arXiv e-prints, arXiv:2308.01230, doi: 10.48550/arXiv.2308.01230
- Maiolino, R., Risaliti, G., Signorini, M., et al. 2024, arXiv e-prints, arXiv:2405.00504, doi: 10.48550/arXiv.2405.00504
- Matthee, J., Naidu, R. P., Brammer, G., et al. 2023, arXiv e-prints, arXiv:2306.05448, doi: 10.48550/arXiv.2306.05448
- Nagao, T., Murayama, T., & Taniguchi, Y. 2001, ApJ, 546, 744, doi: 10.1086/318300
- Natarajan, P., Pacucci, F., Ricarte, A., et al. 2023, arXiv e-prints, arXiv:2308.02654, doi: 10.48550/arXiv.2308.02654
- Nicholls, D. C., Kewley, L. J., & Sutherland, R. S. 2020, PASP, 132, 033001, doi: 10.1088/1538-3873/ab6818
- Oke, J. B. 1974, ApJS, 27, 21, doi: 10.1086/190287
- Osterbrock, D. E. 1978, PhyS, 17, 285, doi: 10.1088/0031-8949/17/3/024
- —. 1989, Astrophysics of gaseous nebulae and active galactic nuclei
- Osterbrock, D. E., & Ferland, G. J. 2006, Astrophysics of gaseous nebulae and active galactic nuclei
- Pacucci, F., & Loeb, A. 2024, arXiv e-prints, arXiv:2401.04159, doi: 10.48550/arXiv.2401.04159
- Pacucci, F., & Narayan, R. 2024, arXiv e-prints, arXiv:2407.15915. https://arxiv.org/abs/2407.15915
- Pacucci, F., Nguyen, B., Carniani, S., Maiolino, R., & Fan, X. 2023, arXiv e-prints, arXiv:2308.12331, doi: 10.48550/arXiv.2308.12331

Peng, C. Y., Ho, L. C., Impey, C. D., & Rix, H.-W. 2002, AJ, 124, 266, doi: 10.1086/340952

- —. 2010, AJ, 139, 2097, doi: 10.1088/0004-6256/139/6/2097
- Pérez-González, P. G., Barro, G., Rieke, G. H., et al. 2024a, arXiv e-prints, arXiv:2401.08782,
 - doi: 10.48550/arXiv.2401.08782
- Pérez-González, P. G., Rinaldi, P., Caputi, K. I., et al. 2024b, ApJL, 969, L10, doi: 10.3847/2041-8213/ad517b
- Planck Collaboration, Aghanim, N., Akrami, Y., et al. $2020,\,A\&A,\,641,\,A6,\,\mathrm{doi}\colon 10.1051/0004\text{-}6361/201833910$
- Reddy, N. A., Kriek, M., Shapley, A. E., et al. 2015, ApJ, 806, 259, doi: 10.1088/0004-637X/806/2/259
- Reddy, N. A., Oesch, P. A., Bouwens, R. J., et al. 2018, ApJ, 853, 56, doi: 10.3847/1538-4357/aaa3e7
- Richards, G. T., Strauss, M. A., Fan, X., et al. 2006, AJ, 131, 2766, doi: 10.1086/503559
- Richstone, D., Ajhar, E. A., Bender, R., et al. 1998, Nature, 385, A14, doi: 10.48550/arXiv.astro-ph/9810378
- Sanders, R. L., Shapley, A. E., Topping, M. W., Reddy, N. A., & Brammer, G. B. 2023, ApJ, 955, 54, doi: 10.3847/1538-4357/acedad
- Scholtz, J., Maiolino, R., D'Eugenio, F., et al. 2023, arXiv e-prints, arXiv:2311.18731, doi: 10.48550/arXiv.2311.18731
- Sérsic, J. L. 1963, Boletin de la Asociacion Argentina de Astronomia La Plata Argentina, 6, 41
- Shen, J., Vanden Berk, D. E., Schneider, D. P., & Hall, P. B. 2008, AJ, 135, 928, doi: 10.1088/0004-6256/135/3/928
- Smith, A., & Bromm, V. 2019, Contemporary Physics, 60, 111, doi: 10.1080/00107514.2019.1615715
- Stern, J., & Laor, A. 2012, MNRAS, 423, 600, doi: 10.1111/j.1365-2966.2012.20901.x

- Tacchella, S., Finkelstein, S. L., Bagley, M., et al. 2022, ApJ, 927, 170, doi: 10.3847/1538-4357/ac4cad
- Thomas, D., Maraston, C., Bender, R., & Mendes de Oliveira, C. 2005, ApJ, 621, 673, doi: 10.1086/426932
- Trussler, J., Conselice, C., Adams, N., et al. 2024, arXiv e-prints, arXiv:2404.07163, doi: 10.48550/arXiv.2404.07163
- Übler, H., Maiolino, R., Curtis-Lake, E., et al. 2023, arXiv e-prints, arXiv:2302.06647, doi: 10.48550/arXiv.2302.06647
- van der Wel, A., Holden, B. P., Zirm, A. W., et al. 2008, ApJ, 688, 48, doi: 10.1086/592267
- van der Wel, A., Chang, Y.-Y., Bell, E. F., et al. 2014, ApJL, 792, L6, doi: 10.1088/2041-8205/792/1/L6
- van Dokkum, P. G., Nelson, E. J., Franx, M., et al. 2015, ApJ, 813, 23, doi: 10.1088/0004-637X/813/1/23
- Wang, B., Leja, J., de Graaff, A., et al. 2024, arXiv e-prints, arXiv:2405.01473, doi: 10.48550/arXiv.2405.01473
- Wang, J.-G., Dong, X.-B., Wang, T.-G., et al. 2009, ApJ, 707, 1334, doi: 10.1088/0004-637X/707/2/1334
- Wild, V., Walcher, C. J., Johansson, P. H., et al. 2009, MNRAS, 395, 144, doi: 10.1111/j.1365-2966.2009.14537.x
- Wild, V., Taj Aldeen, L., Carnall, A., et al. 2020, MNRAS, 494, 529, doi: 10.1093/mnras/staa674
- Williams, C. C., Alberts, S., Ji, Z., et al. 2023, arXiv e-prints, arXiv:2311.07483, doi: 10.48550/arXiv.2311.07483
- Witstok, J., Smit, R., Maiolino, R., et al. 2021, MNRAS, 508, 1686, doi: 10.1093/mnras/stab2591
- Xie, L., Guo, Q., Cooper, A. P., et al. 2015, MNRAS, 447, 636, doi: 10.1093/mnras/stu2487
- Yang, G., Caputi, K. I., Papovich, C., et al. 2023, ApJL, 950, L5, doi: 10.3847/2041-8213/acd639
- Zheng, Z.-Y., Wang, J.-X., Malhotra, S., et al. 2014, MNRAS, 439, 1101, doi: 10.1093/mnras/stu054